SAND2008-3883C

Recent Contributions Of Flame-Sampling Molecular-Beam Mass Spectrometry To A Fundamental Understanding Of Combustion Chemistry

N. Hansen,[a)*] T. A. Cool,[b)] P. R. Westmoreland,[c)] and K. Kohse-Höinghaus[d)]

[a)]*Combustion Research Facility, Sandia National Laboratories, Livermore, CA 94551, USA*
[b)]*School of Applied and Engineering Physics, Cornell University, Ithaca, NY 14853, USA*
[c)]*Department of Chemical Engineering, University of Massachusetts, Amherst, MA 01003, USA*
[d)]*Department of Chemistry, Bielefeld University, D-33615 Bielefeld, Germany*

to be submitted to

Prog Energy Combust Sci

92 Pages

16 Figures

1 Table

[*] Corresponding Author:
Phone: (925) 294-6272, Fax: (925) 294-2276, Email: nhansen@sandia.gov

Abstract

Flame-sampling molecular-beam mass spectrometry of premixed laminar low-pressure flames has been demonstrated to be an efficient tool to study combustion chemistry. In this technique, flame gases are sampled through a small opening in a quartz probe and after formation of a molecular beam, all flame species are detected simultaneously using mass spectrometry. The present review focuses on critical aspects of the experimental approach including probe sampling effects, different ionization processes, and mass separation procedures. Flame-sampling molecular-beam mass spectrometry has greatly benefited from adding the capability of isomer-resolved measurements by employing tunable vacuum-ultraviolet radiation for single-photon ionization, thus facilitating isomer identification. This review also offers an overview of recent combustion chemistry studies of flames fueled by hydrocarbons and oxygenates. The identity of a variety of intermediates in hydrocarbon flames, including resonantly stabilized radicals and closed-shell intermediates, is described, thus establishing a more detailed understanding of the fundamentals of molecular-weight growth processes. Furthermore, molecular-beam mass spectrometric studies of reaction paths in flames of alcohols, ethers, and esters, which have been performed to support the development and validation of kinetic models for bio-derived alternative fuels, are reviewed.

Keywords: low-pressure flame, mass spectrometry, combustion chemistry, aromatic ring formation, oxygenated fuel

1. Introduction

Combustion can be thought of as a self-sustaining reacting flow with temperature and pressure-sensitive reactions, in which chemical energy is converted into heat. From a chemistry perspective, combustion processes are very complex systems, which involve hundreds or even thousands of individual compounds and reactions. These processes usually take place over a wide range of pressures and at temperatures of up to several thousands of kelvins.

Combustion of fossil fuels – coal, oil and natural gas – currently provides about 85% of the energy consumed worldwide. At present, most of the world's transportation energy is supplied by diesel and gasoline-fueled internal combustion engines, which are major contributors of airborne pollutants, including particulate matter (PM, soot), polycyclic aromatic hydrocarbons (PAH), oxides of nitrogen (NO_x), CO, the greenhouse gas CO_2, and unburned volatile hydrocarbon byproducts. Efforts to improve combustion efficiency and to reduce the formation of these pollutants, inherent in the use of petroleum-derived fuels, include improved engine designs, advances in emissions control technologies and the use of cleaner burning fuel formulations. Advances in molecular-level descriptions of combustion processes have contributed to the success of such efforts in recent years.

Two principal themes of current combustion chemistry research have emerged in the past several years. First, while extensive research has yielded a good understanding of NO_x combustion chemistry,[1] soot formation processes are by comparison relatively poorly understood.[2] It is believed however, that PAH's, which themselves pose serious risks to human health,[3, 4] are precursors to soot. As the formation of the first aromatic ring is essential to PAH growth processes, research efforts have focused on the formation routes of benzene and other aromatic species in flames fueled by a variety of different hydrocarbons.[5, 6] Secondly,

dwindling fossil fuel resources and tightened regulations for emissions from internal combustion engines have stimulated a considerable interest in biomass-derived and oxygenated fuels and fuel additives.[7-11] Such alternative fuels not only lower net greenhouse-gas emissions due to their closed carbon cycle and reduce dependence on conventional petroleum, but may also yield reductions in emissions of PAH's when oxygenated fuels are used as replacements for conventional petroleum-based fuels [10, 12-15]. Especially clean-burning renewable oxygenated fuels such as alcohols, ethers, and alkyl esters (biodiesel) are considered to be important replacements for conventional gasoline and diesel fuels.[7-9, 16] Current combustion chemistry research explores the key reaction mechanisms in the oxidation processes of these simple oxygenated compounds.

In general, practical combustion devices are not well suited for direct investigations of complex chemical reaction mechanisms. These devices are turbulent in nature and the description of turbulent flows combined with comprehensive detailed chemical kinetics modeling is still a formidable unsolved problem. The development and validation of kinetic models of combustion chemistry has instead evolved historically from many experimental sources including laminar flame speed measurements, ignition delay measurements and optical detection of species in shock tubes and rapid compression machines, jet-stirred reactor experiments, pyrolysis and oxidation experiments in flow reactors, reaction product sampling with single-pulse shock tubes, species measurements for laminar burner-stabilized flames and co- and counter-flow diffusion flames, and ignition temperature measurements in non-premixed counter-flow diffusion flames. For examples see Refs. [17-21].

The development of flame-sampling molecular-beam mass spectrometry, in use since its inception by Homann, *et al.* in 1963,[22] enables the quantitative detection of both radical and

stable reaction intermediates. The expansion of the flame gases through a quartz nozzle into a lower-pressure region leads to the formation of a molecular beam and allows the detection of virtually all flame species. The sampling technique also allows the selective and sensitive detection of most combustion intermediates without prior knowledge of their identities. Even larger compounds, which are currently not detectable using laser-based diagnostics, can readily be detected and identified. Sampling of gases along the axis of the premixed laminar low-pressure flame results in quantitative mole fraction profiles of all flame species. Such data can then be used to test combustion chemistry models and to determine key reaction pathways. Not until the kinetic models are verified against a range of precise measurements under carefully characterized conditions in a premixed laminar flame, can the models be applied with confidence to more sophisticated practical combustion devices.

Flame-sampling molecular-beam mass spectrometry has had a significant impact on our understanding of fundamental chemical combustion processes in the more than thirty years after publication of Biordi's review paper in 1977.[23] In the past several years, substantial progress has been achieved by supplementing electron-ionization molecular-beam mass spectrometry (EI-MBMS) with isomer-specific measurements using photoionization molecular-beam mass spectrometry (PI-MBMS), employing vacuum-ultraviolet photon beams from synchrotron light sources.[24]

This review concerns itself with the recent experimental progress in flame-sampling molecular-beam mass spectrometry of premixed laminar low-pressure flames and with the unprecedented insights into combustion chemistry gained from flame studies. This article is organized as follows: A comprehensive discussion of the flame-sampling MBMS technique in section 2 is followed with a review of the conclusions from specific studies of flames fueled by

hydrocarbons and oxygenated fuels in section 3. One focus is on newly identified species and their role in aromatics formation and molecular-weight growth processes. In section 4, we draw conclusions and make suggestions for future research.

2. Experimental Section

2.1. Premixed Laminar Low-Pressure Flames

Combustion scientists successfully employ a variety of different model flames in their laboratories.[25] These laboratory flames are generally classified as premixed or non-premixed and laminar or turbulent. In non-premixed flames, the fuel and the oxidizer are initially unmixed, they approach the flame front from opposite sites and mix by molecular diffusion. In a premixed flame, the fuel has been mixed with the oxidizer before they reach the flame front. As a result, the flame speed of premixed flames is limited solely by the chemistry, while in non-premixed flames the speed is predominantly determined by the rates limited by the rates of diffusion.

An example of a premixed laminar low-pressure flame is shown in Fig. 1. The unburned mixture of fuel and oxidizer is delivered to the flame system through a water-cooled burner, typically a large-diameter porous plug made out of stainless steel or bronze. The flame is composed of three regions: a) The preheat zone, which is between the reaction zone and the burner surface, b) the reaction zone, also called luminous zone, which is clearly visible in Fig. 1 as the bright blue zone, and c) the postflame zone, which is the furthest from the burner surface beginning after the reaction zone.

The largest gradients of species concentrations and temperature exist in the preheat zone. As the gas mixture approaches the flame front, it is heated by conduction from the reaction zone and radiation from the reaction and postflame zones. Chemical reactions and heat release are

negligible at this stage; transportation processes, however, play a significant role, i.e., reactants diffuse towards the reaction zone, while intermediates from within the reaction zone diffuse towards the burner surface. Once temperatures are hot enough to sustain combustion, chemical reactions take place in the reaction zone. The thickness of this zone is inversely proportional to the pressure: about 3-10 mm for typical pressures of 10-100 Torr. The gases emerging from the reaction zone enter the postflame zone where only a limited number of reactions take place and the stable combustion products are formed.

Since they are burner-stabilized and premixed, those flames tolerate the physical intrusion of sampling probes, like the one shown in Fig. 1, much better than diffusion flames. By maintaining stable flows and uniform cooling of the burner, a reproducible flame is formed in which radial gradients are negligibly small and species concentrations at a defined position are time-invariant. In this spatially one-dimensional flame, changes need to be followed only as a function of the axial distance from the burner. The stability and quasi one-dimensional structure of laminar premixed flames make them very attractive for laboratory-based investigations of combustion mechanisms and detailed kinetic modeling. However, it should be kept in mind, that in extrapolating results from low-pressure flames to high-pressure conditions, changes in the reaction mechanism may occur.[26]

Typical mole fraction profiles for reactants, intermediates, and products in laminar low-pressure premixed flames are shown together with a typical temperature profile in Fig. 1. Most of the chemical reactions, which are responsible for the heat release or the formation of pollutants, are strongly dependent on the temperature.[5] Therefore, the experimentally determined temperature profiles are a prerequisite for any detailed kinetic modeling of the well-

defined laboratory flames. Accurate methods for temperature measurements are currently based either on laser techniques [27-36] or thermocouples.[37-44]

A key figure for the characterization of flames is the equivalence ratio of a combustion reaction, usually denoted by ϕ. It is defined as the actual starting fuel/oxidizer ratio divided by the ratio required for complete combustion to fully oxidized products, i.e., H_2O and CO_2 for hydrocarbon flames. A stoichiometric flame is specified by $\phi = 1$; leaner or richer conditions are characterized by $\phi < 1$ or $\phi > 1$, respectively. Sometimes the carbon-to-oxygen (C/O) ratio is given in addition to or instead of the equivalence ratio. The C/O ratio is defined as the sum of all carbon atoms involved in the combustion process divided by the sum of all oxygen atoms.

2.2. Flame Sampling And Probe Distortion

A typical probe sampling set-up, which is shown in Fig. 2, consists of a low-pressure (10-100 Torr) flame chamber, a sampling probe, a skimmer, and a detection system, usually some form of mass spectrometer.[23, 45] The purpose of this sampling system is to extract flame gases with a free-jet rapid expansion designed to reach collisionless free-molecular flow on a time scale short compared to that of chemical reactions, thereby "freezing" the chemical composition of the sampled gases to (ideally) closely match unperturbed flame conditions

The sampling probe and skimmer act to create a collisionless molecular beam in two stages. In the first stage free-molecular flow is accomplished by expanding flame gases through a small (250-500 μm) orifice in a quartz probe to a pressure ca. 10^{-4} Torr. A second stage of expansion to a pressure ca. 10^{-6} Torr is provided by a conical skimmer of 1-2 mm aperture, appropriately located in the free-molecular flow region downstream of the sampling probe. The resulting molecular beam enters the ionization region where the species are ionized using

electron- or photoionization techniques. The resulting ions are subsequently separated using a mass spectrometer. The described differentially pumped system is essential, as a low pressure of about 10^{-6} Torr is required for the ionization techniques described in the following section. Quartz is the preferred material for the probe because of its low heat conductivity, its temperature stability, and its chemical inertness.

In comparison with laser based optical diagnostics,[25, 27] which are called "non-intrusive", the flame-sampling techniques are referred to as "intrusive" as the large sampling probe causes variations in the flow field and in the concentration and temperature profiles.[46, 47] For example, it has been found that concentration profiles or radical species determined by mass spectrometry are more sensitive to the probe effects than those of stable species.[46] While heterogeneous recombination of radicals at the probe surface are a likely cause, recombination reactions of radicals on the inner surface of the sampling orifice appears to be negligible. To reduce surface recombination reactions, Biordi *et al.* cleaned the probes by treatment with hot nitric acid solution followed by hydrofluoric acid solution.[45]

Stepowski *et al.* [48] showed with OH LIF that the presence of a quartz nozzle decreases the OH concentration in the preheating zone of the low-pressure C_3H_8-O_2 flame investigated. Downstream of the reaction zone, where the OH concentration gradient is small, no significant perturbations were observed. These effects were explained by a perturbation of the diffusion field by the probe. Smith and Chandler [49] examined the effect of a flame-sampling probe on the structure of a H_2-O_2 flame doped with small amounts of HCN. They used LIF to study the perturbations of the relative CN concentration profile and concluded that both flame chemistry and diffusion play important roles in the observed distortion of the CN profile. In accordance

with the results from Stepowski *et al.,*[48] upstream diffusion blockage of the radical itself seemed to dominate, when sampling close to the burner, where distortions are the largest.

The existence of a thermal perturbation induced by a sampling probe has now been well-established. Probe-induced perturbations of the temperature of up to 500 K have been observed by Pauwels *et al.* [50] in a stoichiometric methanol-air and by Hartlieb *et al.* [36] in a fuel-rich C_3H_6-O_2 flame. Somewhat smaller differences between temperature profiles measured with and without the presence of the quartz probe have been observed for example by Desgroux *et al.*[51] They found distortions of up to 150 K in a low-pressure near-stoichiometric (ϕ = 1.08) methanol-air flame and that the temperature gradient is less pronounced in the reaction zone when the probe is present. Similar differences of approximately 200 K have been observed by Bastin *et al.* in a sooting acetylene flame.[52, 53] All the results indicate that it would be surprising if the rather simple procedure of lowering the unperturbed temperature profile by 100 K [54, 55] would be applicable to flame modeling of a large variety of flames of different fuels, stoichiometries, and pressures.

Related closely to the distortion of the temperature profile is an axial shift of the concentration profiles when sampling within a concentration gradient. In other words, the position from which the sampled gases are drawn is not exactly defined and the calibration of the distance-from-burner axis is difficult to achieve.[56] It appears that the probe is actually sampling flame gases a few orifice diameters upstream of its physical position.[45, 46, 48, 57, 58] Shifting the profiles by a few orifice diameters is a widely accepted correction method.

A quantitative description of the nozzle effects on the flame structure remains currently unfeasible. However, those changes in the flame structure are outweighed by the fact that sampling techniques are the only viable detection methods which allow for the selective and

sensitive detection of all combustion intermediates simultaneously. Biordi *et al.* concluded from their empirical characterization of flame perturbation, that quartz nozzles with an opening angle of ~40° obtain flame data of sufficient quality to permit quantitative analysis.[23, 45]

Another important aspect of the flame-sampling technique is the "temperature" in the molecular beam. Kamphus *et al.* used resonantly enhanced multiphoton ionization (REMPI) measurements on NO and benzene for the characterization of the rotational temperature in molecular beams sampled from premixed laminar low-pressure flames.[59] They found rotational temperatures of 300-400 K virtually independent of the initial temperature. The fact that premixed low-pressure flames typically have Knudsen numbers (ratio of the initial mean free path to orifice diameter) as large as 0.03 probably accounts for the modest cooling and possibly the substantial effects of wall-collisions on the cooling. Measurements of the vibrational temperature or the kinetic energy distribution in the molecular beams have not yet been described. However, the results of Kamphus *et al.* indicate that the expansion does not fall neatly into one of the limiting cases, of either the formation of a supersonic or an effusive molecular beam. Moreover, the dimensions of the flame-sampling part do not vary greatly between different laboratories, therefore, the results of Kamphus *et al.* are likely to be not just peculiar to the instruments employed in their study but of general significance.

2.3. Ionization Processes

After flame gases are sampled through the quartz probe and after the formation of the molecular beam, the flame species are analyzed using mass spectrometry. The first step in the mass spectrometric analysis of the flame-sampled gases is the production of ions from the respective compound. The three different ionization techniques, which are widely used in flame-

sampling studies of low-pressure flames are shown schematically in Fig. 3: electron ionization (EI),[60-62] formerly called electron impact ionization, resonance enhanced multiphoton ionization (REMPI),[63] and single photon ionization.[64]

The experimental result, i.e. the quantitative mole fraction profiles, are independent of the chosen ionization method. In Fig. 4, profiles of benzene in a fuel-rich propene flame (C/O = 0.77, ϕ = 2.3) measured with EI, REMPI, and single-photon PI, are compared. Within the experimental uncertainties, all three ionization methods lead to identical results.

In electron-ionization sources, electrons are produced through thermionic emission by electrically heating a wire filament (tungsten, rhenium or mixtures of thorium and iridium or thorium and rhenium) and subsequently accelerated through the ionization region towards an anode. The radical and molecular flame species are then ionized through interactions with the electrons whose energy exceeds the species' ionization energy (Fig. 3a). It is distinguished between adiabatic and vertical ionization energies. While the adiabatic ionization energy refers to the formation of the molecular ion in its ground vibrational state, the vertical ionization energy applies to the transition of the molecular ion without change in geometry.

For most molecules the probability to get ionized is relatively low if the electron energy is just slightly above the molecule's ionization energy. With larger electron energies the ionization probability increases steadily until it reaches a wide maximum which appears to be around 70 eV. However, all flame species can easily be ionized with energies below 20 eV, thus operating the electron ionization source at 70 eV would likely lead to highly excited ions which would undergo extensive fragmentation. In simple gas mixtures, fragmentation processes may actually be useful as it provides structural information. In flame studies, however, fragmentation is a tremendous problem since one cannot know whether a particular ion signal corresponds to

the molecular ion or from ionization and dissociation of larger molecules. Therefore, most researchers compromise between signal strength and selectivity when they employ electron energies as near to the ionization energy as possible.

The technique of electron-ionization molecular-beam mass spectrometry (EI-MBMS) has been applied successfully for many flame studies, for example Refs. [22, 23, 53, 54, 65-69]. Table 1 lists relevant low-pressure flame measurements of the last 30 years using probe-sampling molecular-beam mass spectrometry.

Besides extensive fragmentation a significant limitation of EI-MBMS is the poor energy resolution of the ionizing electron beam, typically $E/\Delta E < 20$. This low energy resolution is likely to be unsuitable for the determinations of isomeric composition. Instead, photoionization (PI) techniques, such as single-photon ionization [64] and resonance-enhanced multiphoton ionization (REMPI) [63] can be used, since they usually cause less ion fragmentation and offer better sensitivity and selectivity.

With REMPI, the ionization energy is transferred to the molecule with two or more photons (Fig. 3b). It typically involves a resonant single or multiple photon absorption to an electronically excited intermediate state and subsequent absorption of another photon which then achieves ionization of the molecule. Lasers can supply such high photon densities that molecules excited by a first photon may absorb a second one with high probability. In Fig. 3, a commonly used (2+1) REMPI scheme is shown, indicating that two photons are absorbed in the first step and one extra photon is needed for ionization.

An important feature of resonance-enhanced multiphoton ionization is that the excess energy of the photons absorbed in the neutral molecule above the ionization threshold is usually too small to result in fragmentation processes. This so-called “soft ionization” results normally in

totally fragment-free mass spectra. In flame studies, REMPI processes have been greatly used for the detection of aromatic species like benzene, substituted benzenes, and PAH's.[70-78] As an example, the upper trace of Fig. 5 shows a (2+1) REMPI spectrum of toluene in a fuel-rich propene flame. From comparison with a cold gas toluene spectrum (lower trace), it was concluded that this spectrum was produced indeed by toluene.[78] REMPI measurements can also be used for the detection of smaller radicals, like CH_3, which can not be detected by fluorescence techniques.[79]

In the single-photon ionization process, the target molecules are ionized by individual photons whose energy exceeds the molecule's ionization energy (Fig. 3c). To ionize most typical flame intermediates with three or more heavy atoms and most radicals, energies of 6-10 eV are typically required. Most commonly tunable vacuum-ultraviolet (VUV) laser light is generated by two-photon resonance enhanced sum and difference-frequency mixing of dye laser radiation in rare gases and metal vapors as nonlinear medium.[80-82] A very convenient source of 10.5 eV photons is frequency tripling in xenon of the 355-nm third harmonic of Nd:YAG lasers.[83, 84] In principle, VUV laser radiation based on four-wave mixing schemes can cover the full range of 6-19 eV.[85] However, small gaps of low intensities exist in the tuning curve for VUV laser and the use of a tunable VUV laser source to cover a wide energy range as required in many experiments remains difficult and very time-consuming. Nevertheless, laser-based VUV single-photon photoionization has been used to study flame chemistry.[86-93] Happold *et al.* used an ArF laser (193 nm ≡ 6.4 eV) to detect soot precursor compounds in sooting premixed low-pressure C_2H_4-O_2 flames.[94]

Present VUV lasers are not ideally suited for single-photon mass spectrometric studies of flames because of their high intensity, short laser pulse durations, and low repetition rates. The

high laser intensities lead to significant complications from multiphoton ionization and photofragmentation, and the low average powers severely limit the signal-to-noise ratio of photoionization mass spectrometric measurements. These limitations led Cool *et al.* to the design and operation of a flame-sampling molecular-beam mass spectrometer developed for use with synchrotron radiation.[24, 95] A first experiment was set-up at the Chemical Dynamics Beamline of the Advanced Light Source (ALS) of the Lawrence Berkeley National Laboratory, later copied at the National Synchrotron Radiation Laboratory (NSRL) in Hefei, China.[96] The much higher average power of the quasicontinuous synchrotron light yields a typical 200-fold increase in the signal-to-noise ratio for the detection of photoions compared with VUV laser sources. The low intensity of the synchrotron light produces just "soft ionization" without the complications of multiphoton absorption. These capabilities, complemented by the good energy resolution and the tunability of the synchrotron radiation, have been applied to the measurement of isomeric compositions of flame species and some remarkable examples are discussed in section 3 of this review paper. A detailed description of the synchrotron-based PI-MBMS experiments is presented in section 2.6.

2.4. Mass Separation

Once the ions have been produced, they are separated according to their mass-to-charge ratios *m/z*. For flame-sampling mass spectrometric studies, quadrupole mass filters [97] and time-of-flight (TOF) devices [98-101] have been used. These two mass analyzers are best compared by (a) the upper mass limit, which is defined as the highest value of the *m/z* ratio that can be measured, (b) the transmission, which reflects the ratio of the number of ions detected to the number of ions produced in the source, and (c) the mass resolution, commonly defined as

$m/\Delta m$, where m corresponds to m/z and Δm represents the full width of the peak at half maximum. For quadrupoles, the upper mass limit is about m/z = 4000, while linear TOF mass spectrometers have no upper mass limits. Time-of-flight mass analyzers, which measure an entire spectrum at all times, are characterized by their high transmission efficiency, which leads to very high sensitivities. TOF mass spectrometers allow to measure relative peak intensities accurately even though source conditions may vary. However, the most important drawback of the linear TOF analyzers is their poor mass resolution: a maximum of only ~1000 is achievable, compared with ~4000 for quadrupole mass spectrometer.

To improve the mass resolution of time-of-flight instruments, a reflectron is normally used. This device is defined by a series of grids and ring electrodes which create a retarding field that acts as an ion mirror by deflecting the ions and sending them back through the flight tube.[102, 103] The reflectron corrects the energy dispersion of the ions that leave the source. A resolution of $m/\Delta m$ ~3000 for a reflectron TOF mass spectrometer is easily achievable.

An example of a TOF mass spectrum is given in Fig. 6, which shows data from a fuel-rich cyclopentene flame recorded at 2.75 mm distance from the burner at an ionization energy of 11.1 eV.[104] Ions of flame species with mass-to-charge ratios ranging from 15 (CH_3^+) to 92 ($C_7H_8^+$) are detected simultaneously and their signal intensities are correlated to the species' concentrations.

2.5. Electron And Photoionization Cross Sections

For quantitative determinations of flame species mole fraction profiles from the raw mass spectrometric data, absolute photon or electron ionization cross sections are required for each species. Cool *et al.* proposed a data reduction procedure to analyze PI-MBMS data.[105] They

showed that spatial profiles of absolute mole fraction of all flame species are directly measureable when photoionization cross-sections are known over an appropriate range of photon energies.

The ionization cross sections, which express the efficiency for ionization after interactions with electrons or photons, are molecule-specific and a function of the photon or electron energy. It is distinguished between partial and total cross sections. Partial cross sections describe the efficiencies to form a particular ion, while the total cross section is the sum of all partial cross sections. The total absolute number of ionization cross sections is often given in units of a Megabarn (Mb), 1 Mb = 10^{-18} cm^2.

Electron ionization and photoionization cross sections can be measured directly using a gas mixture of known composition which contains the target species and a reference species with a known cross section. Some general trends in electron and photoionization cross sections can be discussed using propane as an example (Fig. 7). For electron ionization, the ionization energy is very difficult to measure, since the thermally generated electrons posses a Gaussian energy distribution (in this case FWHM = 2.4 eV), which creates a rather gradual transition and not a sharp onset at propane's ionization energy. Moreover, above a certain threshold, the ion signal seems to increase monotonically and linearly with the energy of the ionizing electrons.[106, 107] In comparison, single-photon ionization techniques allow an accurate determination of the ionization energy as the photons have a much narrower energy distribution ($E/\Delta E$ ~400 for the synchrotron radiation and $E/\Delta E$ ~10000 for VUV laser sources) – Fig. 7(b). As can be seen in Fig. 7, fragmentation can become an issue above certain electron and photon energies. For electron ionization, the efficiencies with which particular fragments are formed increase monotonically with the electron energy. This behavior is not necessarily evident in

photoionization. For example, the partial cross section of $C_3H_8^+$ seems to reach a plateau above 11.6 eV. Knowledge of these partial photoionization cross sections is of particular importance to account for ion fragments of a given mass-to-charge (*m/z*) ratio that may interfere with the detection of parent-ions of the same *m/z* value. Propane just exemplifies this situation; other combustion intermediates are likely to cause similar interferences that must be considered when species mole fraction profiles are determined. Partial and total cross sections are being measured not just for quantitative mole fraction calculations but also to meet the challenge of properly choosing ionization energies to avoid potential interferences.[108, 109] In some cases, i.e. radical species, it is very difficult to measure accurate ionization cross sections and only a limited number of reliable data is available.[110-112]

The number of experimentally determined electron-ionization cross sections for combustion relevant species is limited. Therefore, theoretical calculations of cross sections appear to be necessary. Predictions of electron-ionization cross sections have largely relied on rather simple additivity rules [113-115] and more rigorous, semi-classical methods like the Deutsch-Märk (DM) formalism [116, 117] and the binary-encounter-Bethe (BEB) method.[118]

Basically two models have been introduced to aim at generating reliable molecular ionization cross sections for photoionization. In Koizumi's model, the total ionization cross section is composed of several spectral components characterized by specific ionization energies.[119] Bobeldijk *et al.* proposed that the molecular photoionization cross section is approximated by the sum of all the cross section of atom pairs.[120]

2.6. Synchrotron Light Sources And PI-MBMS Experiments

In the past several years the PI-MBMS studies of low-pressure laminar flames have greatly benefited from employing tunable, bright vacuum-ultraviolet beams from synchrotron light sources in Berkeley, USA and Hefei, China. Synchrotrons make use of the fact that when charged particles are accelerated, they emit light. For example, electrons can be accelerated to high speed to achieve final energies that are typically in the GeV range. Forcing the electrons then to circle on closed loops in ultrahigh vacuum constitutes an acceleration toward the inside of the curve, and thus the electrons emit radiation.

At the ALS, a 10-cm period undulator beamline [121] is used to provide photon energies ranging from 7.8 to 24 eV under normal 1.9 GeV operation. A gas filter suppresses higher-energy undulator harmonics.[122] A 3-m Eagle monochromator at Endstation 3 of the Chemical Dynamics Beamline delivers about $2\text{-}5\times10^{13}$ photons/s. At NSRL, synchrotron radiation from a bend magnet of a 800 MeV electron storage ring is monochromated with a 1-m Seya-Namoioka monochromator delivering $\sim5\times10^{10}$ photons/s.[123] The working energy resolutions $E/\Delta E$ (FWHM) ~ 250-400 at the Chemical Dynamics Beamline, and $E/\Delta E$ ~500 at NSRL permit estimates of apparent ionization energies with a precision sufficient for the identification of individual isomers of flame species.

The experiments at the ALS in Berkeley and at the NSRL in Hefei provide unprecedented data throughput.[95, 96] The ease with which the photon energy may be precisely tuned near the ionization thresholds for flame species is a feature unmatched by VUV laser and electron sources. Synchrotron based PI-MBMS experiments permit data for a full characterization of a flame to be taken basically within a single day. Selective flames investigated by PI-MBMS are listed in Table 1. Detailed reports of the identification of many species newly detected in flames,

of species mole fraction profiles, and their comparisons to flame models are reviewed in this paper. We therefore introduce the experimental set-ups in Berkeley and Hefei in more detail.

A schematic picture of the molecular-beam sampling apparatus used at the ALS in Berkeley is shown in Fig. 8. A Wiley-McLaren linear (1.3 m) time-of-flight mass spectrometer [99] is used with a mass-resolution of about $m/\Delta m$ ~400 and sensitivity reaching ppm levels.[95] A similar set-up is used at NSRL, however, with modified ion optics. This change potentially reduces the background ion signal, eliminates secondary ionization processes, increases ion detection efficiency, and improves mass resolution. In combination with a reflectron time-of-flight mass spectrometer, a mass resolution of about ~1400 is achieved.[124]

Flame-sampling molecular-beam mass spectrometry with photoionization by tunable vacuum-ultraviolet light enables the detection and separation of isomers based on their unique photoionization spectra. For example, the mole fractions of the two C_3H_4 isomers, propadiene (allene) and propyne, can be determined individually for hydrocarbon flames. The isomers are discriminated against each other according to their different photoionization efficiencies as a function of photon energy (Fig. 9).[24] First, note that although the argon concentration in the investigated flame is over two orders of magnitude larger than those of the minor species at m/z = 40. Essentially no background interference signal is present, demonstrating good suppression of higher energy components of the ALS photon beam. Second, note that the flame-sampled photoionization efficiency (PIE) curve matches the PIE spectrum of allene for photon energies lower than 10.4 eV, the ionization energy of propyne. Above 10.4 eV, both species contribute to the flame-sampled PIE curve. This example shows how photoionization mass spectrometry with bright, easily tunable synchrotron radiation can be used for the unique identification of important intermediates in molecular weight growth. Third, note that the room temperature and flame-

sampled photoionization efficiency spectra can be compared, and that the observed thresholds have been found to be identical in shape within the experimental signal to noise ratios.[24] Possible ionization of hot bands that would lower the apparent ionization energy is negligible. The inset in Fig. 9 shows the isomer-resolved mole fraction profiles of both C_3H_4 isomers.

In Fig. 10(a) the total number of possible isomers of simple hydrocarbons of the general formula C_xH_y are shown. The calculations have been limited to linear molecules and ring structures with more than 4 C-atoms. Needless to say, most of the theoretically conceivable structures are not likely to be detected in flames, however, it is obvious that the total number of isomers increases exponentially with the molecular size. Figure 10(b) shows a two-dimensional plot of the ionization energies of several species with near or equal masses which can be separated by their characteristic ionization energy. Some generally considered flame species in the mass range from 40 (allene and propyne) to 78 (fulvene and benzene) with ionization energies between 8 and 11 eV are shown. For example, at m/z = 44, ethenol (CH_2CHOH) and acetaldehyde (CH_3CHO) can easily be separated.[125, 126] Further examples will be discussed in section 3.

These PI-MBMS instruments are configured to collect data in two modes. In the first, the photon energy is fixed, and the burner is scanned to produce mass spectra at each burner height, or in the second, the burner height is fixed and the photon energy is scanned to record photoionization efficiency spectra.[95, 127] The first data is subsequently analyzed to produce species mole fraction vs. burner height profiles for comparison to models, while the second mode is essential to identify species by their ionization threshold as well as their mass.[24, 125, 128, 129] In favorable cases multiple species at a single m/z ratio have been identified by observing multiple thresholds.

3. Flame Chemistry

The quantitative flame-sampled mass spectra and temperature profiles are subsequently used to improve combustion chemistry models. For example, flame data has been used to extract rate constants of several important reactions.[130-135] Significant advances were also made by identifying key combustion intermediates, thus allowing the elucidation of fundamental reaction paths. In this section, recent MBMS studies focusing on the understanding of the formation of aromatic species and their growth to PAH's and soot are discussed. Furthermore, flame-sampling MBMS work concerning the combustion chemistry of oxygenated fuels, e.g. alcohols, ethers, and esters, is reviewed.

3.1. Hydrocarbon Flames

3.1.1. Resonantly Stabilized Radicals In Aromatic Ring Formation

It is now well accepted that small, unsaturated hydrocarbon radicals, particularly resonantly stabilized ones, are critical elements of the gas-phase chemistry that first lead to aromatic species and ultimately to soot formation in rich flames.[2, 5, 136] These resonantly stabilized radicals are characterized by multiple electronic structures corresponding to the same nuclear structure. That is, at least one unpaired electron is delocalized and spread out over two or more sites in the radical. Resonantly stabilized radicals are thermodynamically more stable than non-resonantly stabilized radicals. Their larger formation and slower destruction rates compared with non-resonantly stabilized radicals, result in higher concentrations.[5] From the combustion chemistry point of view, the most important resonantly stabilized radical is propargyl (C_3H_3), $\bullet CH_2\text{-}C{\equiv}CH \leftrightarrow CH_2{=}C{=}\bullet CH$. Its reactions with another propargyl or with an allyl (C_3H_5)

radical are the most commonly proposed cyclization steps and are believed to be the main source of the "first aromatic ring" in flames burning aliphatic fuels and the rate-limiting steps in soot formation processes.[5, 136-139]

However, a number of other reactions, including isomers of C_3H_2, C_4H_3, C_4H_5, C_5H_3, and C_5H_5 have been considered as possible cyclization steps.[2, 5, 6] The isomeric composition of those radicals has been elucidated in recent years by PI-MBMS studies of low-pressure flames in combination with high-level *ab-initio* calculations. The results are reviewed in the following paragraphs.

C_3H_2: Possible isomers of C_3H_2 are shown in Fig. 11. The singlet-cyclopropenylidene (*cyclo*-$^1C_3H_2$) is the energetically most stable C_3H_2 isomer, while triplet-propargylene (^{3}HCCCH) is the second most stable form, with ca. 11 kcal mol^{-1} higher energy. The singlet state of propadienylidene (^1H_2CCC) lies another 2 kcal mol^{-1} higher than ^{3}HCCCH.[140-142] Miller and Melius suggested that ^{3}HCCCH could react with C_3H_3 to form phenyl, thus providing a conceivable cyclization step.[136] An accurate flame model analysis of the role of C_3H_2 in flame chemistry requires a reliable characterization of its isomeric distribution. However, flame-sampled data from laminar low-pressure flames using electron-ionization did not permit distinction among several C_3H_2 isomers.[142, 143] Using photoionization mass spectrometry with tunable vacuum-ultraviolet synchrotron radiation, Taatjes *et al.* studied the isomeric composition of C_3H_2 sampled from a fuel-rich cyclopentene flame.[142] The comparison of the experimental photoionization efficiency spectra with simulated Franck-Condon envelopes suggests the presence of both ^{3}HCCCH and *cyclo*-$^1C_3H_2$.

Taatjes *et al.* concluded that the presence of ^{3}HCCCH is probably a consequence of the reaction of hydrogen atoms with propargyl.[142] The energetically most stable *cyclo*-$^1C_3H_2$ is

the least favored product in that reaction, however, it can be formed through collisional rearrangement of various singlet isomers, namely ^1H_2CCC, ^1HCCCH and *cyclo*-^1HCCCH, which are formed in minor channels.[144]

C_4H_3 and C_4H_5: There has been a longstanding debate regarding the possible importance of the C_4H_3 and C_4H_5 radicals in ring-formation processes. The C_4H_3 and C_4H_5 isomers widely considered in combustion models are shown in Fig. 11. The *n*-isomers of C_4H_3 and C_4H_5 ($\bullet$CH=CH-C≡CH and $\bullet$CH=CH-CH=CH_2) are not resonantly stabilized and are less stable by about 12 kcal mol^{-1} than the corresponding resonantly stabilized *i*-isomers (CH_2=$\bullet$C-C≡CH ↔ CH_2=C=C=$\bullet$CH and $\bullet CH_2$-CH=C=CH_2 ↔ CH_2=CH-$\bullet$C=CH_2).[136, 145-147] For C_4H_5, there are two additional resonantly stabilized isomers to be considered in flame chemistry: CH_3-$\bullet$C=C=CH_2 ↔ CH_3-C≡C-$\bullet CH_2$ (1-methyl-allenyl) and CH_3-$\bullet$CH-C≡CH ↔ CH_3-CH=C=$\bullet$CH, both of which can be considered as methyl-substituted propargyl radicals.

Especially the additions of C_2H_2 (acetylene) to the *n*-C_4H_3 and *n*-C_4H_5 isomers have been proposed as an important cyclization step under combustion conditions.[2, 6, 148-152] Westmoreland *et al.*,[153] Wang and Frenklach,[149] and Senosiain and Miller[154] have analyzed the potential energy surfaces for those reactions. It is shown that these reactions do not require any H-atom transfers from one C-atom to another and that the additions to the *n*-isomers have lower-energy barriers than those for the corresponding reactions of the *i*-isomers.[136, 154, 155] However, Miller and Melius [136] and Klippenstein and Miller [156] pointed out that thermochemistry and formation chemistry favor *i*-C_4H_5 and that the concentrations of *n*-C_4H_3 and *n*-C_4H_5 are simply too small for their reactions with acetylene to be effective benzene formation pathways. In high-temperature reaction zones of rich flames, *n*-C_4H_5 can be easily converted to the more stable *i*-isomer by H-atom assisted isomerization.[5, 136]

Hansen *et al.* identified C_4H_3 and C_4H_5 isomers in fuel-rich allene, propyne, cyclopentene, and benzene flames by combining synchrotron-based PI-MBMS studies with *ab initio*-based Franck-Condon simulations.[145] On the basis of calculated ionization energies, frequencies, and force constants, the Franck-Condon analysis suggests that mostly *i*-C_4H_3 is detected at *m/z* = 51 and that *i*-C_4H_5, CH_3CCCH_2, and/or CH_3CHCCH isomers are present at *m/z* = 53. Potentially rather small amounts of *n*-C_4H_3 and *n*-C_4H_5 together with large differences in vertical and adiabatic ionization energies made it difficult to detect those isomers.

The detection of the *i*-C_4H_3 and *i*-C_4H_5 isomers points out clearly that their reactions with acetylene deserve testing in chemical kinetics flame modeling. Indeed, Walch showed previously that the *i*-$C_4H_3 + C_2H_2$ reaction would yield phenyl (or *o*-benzyne + H),[155] while Miller and Melius suggested that the reaction of *i*-C_4H_5 with acetylene was a plausible cyclization step under certain flame conditions.[136] Senosiain and Miller concluded from their theoretical study that although the rate coefficient for *n*-$C_4H_5 + C_2H_2$ is considerably larger than that for *i*-$C_4H_5 + C_2H_2$, it is the latter reaction that plays the more important role in flame chemistry.[154] This conclusion is largely based on the very fast H-atom assisted isomerization of the *n*-isomers to the *i*-forms. The *i*-$C_4H_5 + C_2H_2$ reaction forms fulvene + H without undergoing any H-atom transfers or going through any multi-centered transition states after the initial complex is formed. Subsequently, the fulvene produced is relatively easily converted to benzene by H-atom assisted isomerization.[157]

The role of the newly identified methyl-substituted C_4H_5 isomers (CH_3CCCH_2 and/or CH_3CHCCH) in ring formation processes requires further investigation. CH_3CHCCH appears to be completely absent from current flame models. However, the reactions $CH_3CCH_2 + C_3H_3$ and $CH_3CCH_2 + CH_3CCH_2$ could form benzyl + H or toluene and *o*-xylene, respectively, through a

sequence of steps analogous to those by which $C_3H_3 + C_3H_3$ reaction form benzene and phenyl + H.[137, 139, 158]

C_5H_3 and C_5H_5: In a study related to the identification of the C_4H_3 and C_4H_5 radicals in fuel-rich flames, Hansen *et al.* used an identical approach to identify C_5H_3 and C_5H_5 isomers.[128] For C_5H_3, the presence of both the $H_2CCCCCH$ (*i*-C_5H_3) and the HCCCHCCH (*n*-C_5H_3) isomers was revealed. Electronic structures for the resonantly stabilized *i*- and *n*-C_5H_3 radicals are shown in Fig. 11. C_5H_5 was identified as mainly *cyclo*-C_5H_5 (cyclopentadienyl radical), although some small signal was detected below its characteristic ionization energy of 8.4 eV.[128] Contributions from the resonantly stabilized linear *l*-C_5H_5, $CHCCHCHCH_2$, have been later identified by Yang *et al.*[159]

The role of C_5 radical species in molecular weight growth processes is largely uncertain. By far the most important resonantly stabilized C_5 radical is *cyclo*-C_5H_5 (cyclopentadienyl radical), which has been widely accepted to form naphthalene through a self-recombination reaction,[2, 5, 6, 139, 157, 160] or to form fulvene through reaction with methyl radicals.[157, 161, 162] As a consequence, cyclopentadienyl is believed to be an important intermediate in the growth of higher hydrocarbons, PAH, and soot in rich flames. Based on electronic structure calculations of Mebel *et al.*,[163] Pope and Miller suggested that the reaction of the resonantly stabilized *i*-C_5H_3 ($H_2CCCCCH$) with CH_3 could be partially responsible for benzene formation.[138] Both *i*- and *n*-C_5H_3 isomers are substituted propargyl radicals. Analogous to the propargyl recombination and similar reactions proposed for 1-methyl-allenyl (CH_3CCCH_2), *i*-C_5H_3 could undergo reactions with radical-substituted propargyl ($RCCCH_2$) radicals or propargyl (R = H) to form phenylacetylene (C_6H_5CCH), methyl-substituted phenylacetylene (CH_3-C_6H_4-CCH), or diethynylbenzene (HCC-C_6H_4-CCH).

3.1.2. Isomer-Resolved Measurements Of Various Combustion Intermediates

Besides for those key radical species, the isomeric identity has been resolved for a variety of closed-shell, stable, intermediates in hydrocarbon flames employing the synchrotron PI-MBMS technique. Within the series of C_4H_x (x = 4,6, and 8) several isomers have now been unambiguously identified and can be determined quantitatively. For example, butatriene, CH_2=C=C=CH_2, the cumulenic isomer of the well-known intermediate vinylacetylene, CH_2=CH-C≡CH, has been observed in flames fueled by hydrocarbons.[104, 164-166] For C_4H_6, contributions from 1,3-butadiene (CH_2=CH-CH=CH_2), 1-butyne (CH≡C-CH_2-CH_3), and 2-butyne (CH_3-C≡C-CH_3) have been separated based on their different ionization energies, as seen in Fig. 10(b).[104, 166] In a similar fashion, contributions from 1-butene (CH_2=CH-CH_2-CH_3), 2-butene (CH_3-CH=CH-CH_3), and acrolein (CH_2=CH-CHO) to signal at *m/z* = 56 have been seperated.[104, 127, 166] Interestingly, 1-butene, which is a potential product of the reaction of allyl with methyl radicals, was found to be present in stoichiometric and fuel-rich allene flames but not in flames fueled by its isomer propyne.[127, 166]

According to Fig. 10(a), there are generally more isomers to be considered for C_5 intermediates than for C_4 species. A variety of different closed-shell isomers of C_5H_4, C_5H_6, and C_5H_8 may appear in fuel-rich hydrocarbon flames. For example, the observed flame-sampled photoionization efficiency spectrum for C_5H_4 in combination with *ab-initio* calculations revealed the presence of CH_2=C=C=C=CH_2, CH_2=C-CH-C≡CH and CH_3-C≡C-C≡CH.[128] The presence of the latter two isomers can be expected, as they are thought to be reaction products of C_2H with allene and propyne, respectively.[167, 168] Analogous reactions of C_4H with allene, propyne, and vinylacetalene have been proposed to explain the observation of the corresponding C_7H_4 and

C_8H_4 polyynic intermediates.[169] The role of the C_5H_4 isomers in molecular-weight processes is not immediately obvious. However, by H-abstraction reactions, *n*-C_5H_3 and *i*-C_5H_3 are formed, potentially followed by ring-forming reactions as discussed in the previous section. An interpretation of the observed flame-sampled photoionization efficiency spectra is becoming more difficult for C_5H_6 and C_5H_8. However, contributions from cyclopentadiene, CH_3-C≡C-CH=CH_2, CH_3-CH=CH-C≡CH, and CH_2=CH-CH_2C≡CH were observed for C_5H_6 in model flames fueled by allene, propyne, cyclopentene, or benzene. Cyclopentene, CH_2=CH-CH-CH-CH_3, CH_3-C≡C-CH_2-CH_3, and CH_2=CH-CH_2-CH=CH_2 were found to contribute to the C_5H_8 signal.[128]

Besides the isomer-specific measurements of various C_6H_6 precursors, the qualitative and quantitative determination of different C_6H_6 isomers is also of paramount interest for our understanding of flame chemistry. The lower ionization energy of fulvene (8.36 eV) compared with benzene (9.25 eV) – see Fig. 10(b) – allows distinctive determination of mole fraction profiles of both species independently.[104, 123, 166, 170-173] However, it should be kept in mind, that the presence of other C_6H_6 isomers with ionization energies between 8.36 and 9.25 eV is impossible to be verified as long as the photoionization efficiency curve of fulvene is unknown. Law *et al.* believed to detect 1,5-hexadiyne (HC≡C-CH_2-CH_2-C≡CH) in a fuel-lean ethylene flat flame doped with allene.[174] However, its presence was later not confirmed in pure allene and propyne flames.[166]

Various C_7 species, including toluene, ought to be considered in molecular-weight growth processes in fuel-rich flames. High-level *ab-initio* calculations combined with flame-sampling PI-MBMS employing synchrotron generated VUV photons were used to identify C_7H_6 and C_7H_8 isomers, pointing towards the existence of C_5-C_7 ring enlargement reactions.[175]

Hansen *et al.* confirmed the presence of the five-membered C_5H_5CCH or $C_5H_4CCH_2$ and cycloheptatriene.[104] From the chemical point of view, the C_7H_6 isomers are likely to be formed by the reactions summarized schematically in Fig. 12: (a) The initial adduct of the $C_5H_5 + C_2H_2$ reaction can undergo an exothermic 1,3-hydrogen shift to recover the stability of the "parent" resonantly stabilized C_5H_5 ring and to form the $C_5H_4CHCH_2$ radical. It seems plausible that the $C_5H_4CCH_2$ isomer is subsequently formed by hydrogen loss or abstraction. (b) In the hydrogen-rich environment of a fuel-rich flame it is furthermore conceivable that hydrogen atom migration around the cyclopentadiene ring takes place to convert the initial isomer into the most stable -$CH_2CHCHCHC(CCH)$- tautomeric species. (c) The initial C_7H_7 radical can undergo isomerization to form the resonantly stabilized cycloheptatrienyl and benzyl radicals, subsequently forming cycloheptatriene and toluene.[175, 176] The C_7H_7 radical species are quite stable and thus they are good precursor candidates for forming multiring structures, including indene and naphthalene.[160, 176, 177] The newly identified flame species and the described reactions, leading from C_5 to C_9 or C_{10} species through C_7 intermediates, reveal a molecular growth path through C_5-C_7 ring enlargement reactions.

Several problems arise when interpreting observed flame-sampled photoionization efficiency spectra of large species: a) As mentioned above, the total number of isomers increases exponentially. b) More isomers are becoming potentially important as differences in heats of formation decrease. c) Similar structural features of the isomers can result in almost identical ionization energies and undistinguishable photoionization efficiency spectra. d) Ionization energies of all conceivable isomers are not known completely and need to be either measured or calculated employing quantum chemistry. e) Photoionization efficiencies are not as well known as for smaller combustion intermediates. Consequently, contributions from isomers with

ionization energies above the observed threshold can not be ruled out completely. Regardless of those severe problems, the NSRL group characterized a variety of high-mass species in a series of different low-pressure flames fueled by hydrocarbons and by gasoline.[123, 164, 170, 171] Obviously, these first assignments could not been based on the observed photoionization efficiencies and ionization thresholds alone, but also on current chemical understanding.

3.1.3. Experimental and Modeling Flame Studies Of Benzene Formation

Species identification, as described in the previous sections, can just be the first step to further deepening the current understanding of combustion processes. In a second step, flame modeling based on detailed chemical kinetic mechanisms should be applied to elucidate the importance of various reactions. In the last years, experimental MBMS data from premixed laminar low-pressure flames have been extensively used to investigate formation routes to aromatic species.

Numerous MBMS studies exist on premixed laminar low-pressure flames fueled by methane [132, 178-183] and the C_2 species acetylene [77, 133, 153, 184, 185], ethylene [55, 130, 165, 179, 186, 187], and ethane.[134, 181-183] Pope and Miller [138] chose data from premixed laminar low-pressure flames fueled by acetylene,[188] ethylene,[130] and propene [189] to explore benzene formation pathways. They concluded that in all three flames, the only major formation pathways for benzene or phenyl were the result of combination of C_3 radicals, i.e. propargyl + propargyl and propargyl + allyl. Contributions from addition of C_4 radicals to C_2H_2 appeared to be not significant. In a related study, Richter and Howard [190] confirmed propargyl recombination to be the dominant benzene formation pathways in fuel-rich acetylene [153, 191] and ethylene [130] flames. For the acetylene flame, this observation has been verified later by

Rasmussen *et al.*,[192] who estimated a high-temperature, low-pressure rate constant for the propargyl recombination from the flame measurements. Richter and Howard's conclusion that the reactions of *n*-C_4H_3 and *n*-C_4H_5 with C_2H_2 are found to play no significant role in the formation of single-ring aromatics in both flames refutes earlier modeling studies by Wang and Frenklach for the same acetylene flame.[148] These models could now be compared with new experimental data sets of a rich acetylene flame by Lamprecht *et al.* [184] or an isomer-specific data set of a stoichiometric ethylene flame from Zhang *et al.*[165] Results of Delfau and Vovelle have shown that polyacetylenic hydrocarbons cannot be considered as active intermediates responsible for the formation of soot in C_2H_2-O_2 flames.[193]

The above-mentioned propargyl + propargyl recombination reaction was also found to be the dominant source of benzene in rich flames fueled by propene (C_3H_6).[68, 74, 77, 184, 189] Besides C_3H_6, two isomeric forms of C_3H_4, i.e. allene (CH_2=C=CH_2) and propyne (CH_3-C≡CH) have been used as fuels in premixed laminar low-pressure flames to investigate benzene formation routes. Law *et al.* [174] added small amounts of allene to a fuel-lean ethylene flat flame and performed both EI- and PI-MBMS experiments. The modeling of that flame suggested that the C_3H_3 recombination reaction is the major formation pathway of benzene. This study was followed by an accurate PI-MBMS experiment and detailed modeling of rich flames fueled by only allene or propyne.[166] These allene and propyne flames are of considerable interest because both isomers lead immediately to the propargyl radical, that is, in rich flames, both fuels are consumed by hydrogen abstraction: C_3H_4 (allene or propyne) + H ⇄ C_3H_3 + H.

The temperature profiles and mole fraction profiles for major species were found to be quite similar for the isomeric fuels, as illustrated in Figs. 13(a) and (b). This observation supports the feasibility to elucidate fuel-specific reaction pathways when using isomeric fuels. This

approach allowed for the identification of isomeric differences in both flames and for the tracking of the H-assisted conversion from allene to propyne and from propyne to allene: C_3H_4 (allene) + H ⇄ C_3H_4 (propyne) + H.[194] The experimental and modeled profiles of allene in the propyne flame and propyne in the allene flame are shown in Figs. 13(c) and (d). It can be seen that more propyne is formed in the allene flame than allene is formed in the propyne flame. This can be understood in light of the slightly higher thermodynamic stability of propyne and the dissociation of propyne: C_3H_4 (propyne) + H ⇄ CH_3 + C_2H_2. As a consequence, less propyne can be converted into allene. This dissociation reaction is also responsible for the observed smaller propargyl concentration in the propyne flame than in the allene flame. Figures 13(c) and (d) compares experimental results for C_3H_3 with the modeling results and an excellent agreement is observed. The smaller propargyl concentration in the propyne and the larger concentration of allyl in the allene flame (allyl can be directly formed from allene but not from propyne by H-addition) lead ultimately to smaller concentrations of benzene in the propyne flame, as seen in Figs. 13(e) and (f). The slight overprediction of the mole fraction of benzene in the models for both flames indicates the use of a rate constant for propargyl + propargyl recombination which is too fast.[137]

Recently, the focus of combustion research has shifted from those small (C_1-C_3) hydrocarbons towards larger, more complex hydrocarbons that are found in most liquid fuels.[6] For example, larger alkenes are constituents of engine fuels and are also important intermediate species in the dehydrogenation process of the parent alkanes. The benzene formation chemistry in flames fueled by 1,3-butadiene has attracted some attention.[150, 195, 196] Cole *et al.* [150] and Hansen *et al.* [196] used the EI- and PI-MBMS techniques, respectively, to map the composition of rich flames. The latest modeling suggested that propargyl + propargyl and

contributions from *i*-C_4H_5 + C_2H_2 contribute to the benzene formation.[196] In an experimental and modeling study of 1-pentene (CH_2=CH-CH_2-CH_2-CH_3) combustion at fuel-rich conditions, González Alatorre *et al.* [197] concluded, that the fuel decomposes easily to form C_3 and C_2 fractions. Consequently, the dominant pathway for benzene formation was inferred to be the recombination of propargyl radicals.

In view of the potential importance of C_5 species, e.g. naphthalene or benzene formation through reactions of *cyclo*-C_5H_5,[2, 5, 6, 138, 157, 177, 198] studies of cyclopentene (*cyclo*-C_5H_8) flames are of significant interest. The fuel cyclopentene is attractive for studies because the abstraction of hydrogen atoms forms cyclopentadienyl radicals, thus, in this flame the importance of C_5 intermediates should be enhanced compared to C_3 species. However, a modeling study of an EI-MBMS measurement of Lamprecht *et al.* [199] indicated that benzene (and fulvene) formation are dominated by the propargyl + propargyl self-combination with only minor contributions from the *cyclo*-C_5H_5 + CH_3 reaction.[200] This result can be understood in light of the easy formation of propargyl radicals in cyclopentene flames, as they are readily formed as a decomposition product of *cyclo*-C_5H_5 radicals: *cyclo*-C_5H_5 ⇄ *linear*-C_5H_5 ⇄ C_2H_2 + C_3H_3. The importance of propargyl recombination in cyclopentene flames was later confirmed by Kamphus *et al.* modeling REMPI-MBMS experimental results of a rich cyclopentene flame.[74] Other pathways leading to benzene or phenyl + H, i.e. C_4H_x + C_2H_2 and C_5H_3 + CH_3 have been found to be of little or no importance. A fuel-rich flame of 1,3-pentadiene (CH_2=CH-CH=CH_2-CH_3), an isomer of cyclopentadiene, has been investigated by Atakan *et al.* employing EI-MBMS.[201] According to their analysis, pathways including C_3 species (C_3H_3 + C_3H_3 and C_3H_3 + C_3H_5) are dominant pathways towards C_6H_6 in a 1,3-pentadiene flame.

However, they point out that reactions of C_2H_2 with C_4H_5 and of *cyclo*-C_5H_5 with CH_3 may be relevant as well.

Although the critical role of resonantly stabilized radicals has been emphasized in the literature [5, 136-138, 158] and in the previous sections and paragraphs, those reactions do not need to dominate necessarily. In an experimental and modeling study of a stoichiometric cyclohexane flame, Law *et al.* found that benzene is formed largely be dehydrogenation of cyclohexane through cyclic intermediates.[202] This process is shown schematically in Fig. 14. The 1,3-cyclohexadiene has been unambiguously identified in their work, while no evidence of the 1,4-isomer has been found. Measured burner profiles of C_6H_{12}, C_6H_{10}, C_6H_8, and C_6H_6, in combination with a fulvene-to-benzene ratio much smaller than expected from propargyl + propargyl recombination, suggest the importance of the cascading dehydrogenation. Parallel modeling studies by Zhang *et al.* [203, 204] and Silke *et al.* [205] propose generally similar ideas of benzene formation via dehydrogenation. Especially, the detailed modeling in Ref. [204] of the flame reported by Law *et al.,*[202] provided a detailed insight into the major reaction pathways, fuel consumption, and benzene formation.

3.1.4 Flame Chemistry Beyond The First Aromatic Ring

Growing concerns about negative health effects of combustion generated compounds and particles motivated the investigation of molecular-weight growth processes in flames. For studies of the formation of polycyclic aromatic hydrocarbons (PAH's) in flames, it is advantageous to use a fuel that produces these compounds in sufficient concentrations, e.g. aromatic species like benzene. Naphthalene, the smallest PAH, was used as a fuel by Homann and coworkers to study the formation of large molecules, including fullerene and small soot particles.[70, 206, 207]

Benzene is currently assumed to be one of the most important soot precursors in rich hydrocarbon flames.[208] It is therefore not surprising that flames by benzene have been described experimentally and theoretically in numerous publications, starting with the pioneering work of Bittner and Howard.[54] Several detailed kinetic modeling studies are based on the experimental mole fraction profiles of the $\phi = 1.8$ flame presented in their work.[190, 209-214]

Isomer-specific results from two very similar benzene-oxygen flames have been reported by Qi *et al.* ($\phi = 1.66$) and Yang *et al.* ($\phi = 1.78$),[123, 164] employing tunable synchrotron photoionization molecular-beam mass spectrometry. They matched observed ionization thresholds with known ionization energies of several isomers to identify key combustion intermediates. However, as mentioned above, especially for the larger molecules, the assignment to just one isomer can be not more than a first guess, since other isomers, with larger ionization energies, can no be ruled out completely. Nevertheless, their extensive list of species and their mole fraction profiles build a useful foundation for more detailed modeling. Compared to the studies by Bittner and Howard,[54] the NSRL group found a number of new isomers. Taking the newly observed intermediates into consideration probably leads to a significant advancement of the modeling efforts. Defoeux *et al.* [215] used EI-MBMS to detect profiles of species up to $C_{22}H_{12}$ in a fuel-rich ($\phi = 2.0$) benzene-oxygen flame. They saw a substantial increase in the maximum concentrations of PAH's when comparing their data with the somewhat leaner flame ($\phi = 1.8$) studied by Bittner and Howard.[54]

A $\phi = 2.0$ benzene-oxygen flame at low pressure was also investigated by Homann and coworkers.[71, 72, 76] They combined molecular-beam sampling with REMPI and time-of-flight mass spectrometry to study the formation of PAH's with 18-70 carbon atoms per molecule. Up to $C_{24}H_{12}$, they observed a nearly exponential decrease in PAH concentrations with increasing

number of C atoms. This decrease is followed by an increase in concentration up to about C_{50} and a subsequent smooth decrease to still larger species.

Fuel-rich combustion is widely used for the synthesis of carbonaceous material, including fullerenes.[73, 216-219] However, flame-sampling techniques as described in this review article are likely not to be suited to investigate sooting flames as the small particles tend to clog the small opening in the quartz sampling probe.

In somewhat related studies, Huang *et al.* [170] and Li *et al.* [171] studied fuel-lean and rich gasoline-oxygen flames using VUV photoionization MBMS. However, because of the complex composition of the gasoline fuel,[220] the amount of unambiguous results on flame chemistry is limited. Nevertheless, their work represents an important first step to identify combustion intermediates in flames of practical fuels.

3.2. Oxygenated Flames

In recent years, the studies of hydrocarbon flames with molecular-beam mass spectrometric sampling techniques have been complemented by studies of flames of oxygenated fuels. As discussed in the Introduction, the pronounced interest in those alternative fuels stems mostly from environmental and health concerns of the emissions from internal combustion engines. Flame-sampling molecular-beam mass spectrometry can help to understand the oxidation chemistry of small alcohols, ethers, and model esters. It is also useful to identify key chemical reaction mechanisms responsible for the observed reductions in polycyclic aromatic hydrocarbons, particulate matter, unburned hydrocarbons, and carbon monoxide when oxygenated fuels are used.

3.2.1. Combustion Chemistry In Flames Fueled By Alcohols, Ethers, And Esters

Alcohols: There has been some considerable interest to use alcohols, especially methanol and ethanol, as alternatives to conventional fuels. Methanol, CH_3OH, is the simplest alcohol and it can be used as a possible fuel for engines. It is advantageous over petroleum based conventional fuels because of a lower ignition delay, a higher burning velocity and reduced propensity to knock.[7] However, only a few fundamental combustion studies in premixed laminar low-pressure flames are reported. Especially methanol-air flames have been investigated by a variety of different techniques, including electron-spin resonance (ESR),[50, 221, 222] flame-sampling with subsequent gas chromatographic analysis,[50, 223, 224] and EI-MBMS.[225] This technique was also employed by Vandooren and van Tiggelen to study fuel-lean low-pressure methanol-oxygen and methanol-hydrogen-oxygen flames,[226] which subsequently have been examined mechanistically.[227] Detailed information on the principal paths of methanol consumption and deduced rate constants for reactions involved in the oxidation of methanol were reported. The combustion chemistry of methanol is fairly straightforward: It converts easily to formaldehyde (CH_2O) and subsequently to CO.[228, 229]

Ethanol (C_2H_5OH), the second smallest alcohol, is widely used as a transportation fuel in internal combustion engines. It is used as a fuel extender for petroleum-derived fuels and as an octane enhancer.[230] Ethanol is mainly produced from renewable biomass resources; its use can potentially balance the emission of carbon dioxide. The consumption of ethanol as an alternative fuel is supposed to increase the next few years, thus warranting a critical evaluation of its combustion chemistry.

Surprisingly, there are only few data available on ethanol flame structures. Tanoff *et al.* used continuous microprobe sampling followed by electron-ionization mass spectrometry from a fuel-lean ethanol-oxygen flame to measure reliable concentrations of reactants, products, and

some intermediates.[231] Kasper *et al.* investigated two ethanol-oxygen flames with stoichiometries of $\phi = 1.00$ and $\phi = 2.57$ by EI-MBMS.[75] All major species and families of hydrocarbon and oxygenated species in the C_1-C_3 range were detected in the pure ethanol flames and absolute mole fractions were determined. Concentrations of the propargyl radical have been above the detection limit only in the fuel-rich flame, while they have not been detected in the stoichiometric flame. Benzene was below the detection limit in both ethanol flames using EI-MBMS, however it was detected using REMPI-MBMS in the rich flame. Leplat *et al.* combined EI-MBMS measurements of a low-pressure stoichiometric ethanol flame with kinetic modeling to deduce main consumption pathways in ethanol combustion.[232] In their study, the models of Dunphy *et al.,*[233] Norton and Dryer,[234] Dagaut *et al.,*[235] and Marinov [236] have been used, resulting in a good agreement for only the main species profiles.

The early fuel-consumption pathways of ethanol are shown schematically in Fig. 15. Oxidation is typically initiated by hydrogen abstraction, which in the case of ethanol can occur at three reaction sites, leading to the formation of 3 different C_2H_5O radicals. Although all pathways are likely to occur, the formation of the CH_3CHOH radical is preferred because the CH bond at the α-carbon is the weakest. As indicated in Fig. 15, the C_2H_5O radicals are subject to subsequent β-scissions to form a stable molecule and a radical species. Ethene, ethenol, acetaldehyde and formaldehyde are thus readily formed in ethanol oxidation processes.

The situation is becoming more complex for C_3 and C_4 alcohols. Propanol exists in two isomeric forms, the *n*-propanol ($CH_3CH_2CH_2OH$) and the *iso*-propanol ($CH_3CHOHCH_3$), in addition, there are a total of four different isomers of butanol, 1-butanol ($CH_3CH_2CH_2CH_2OH$), 2-butanol ($CH_3CH_2CHOHCH_3$), *iso*-butanol ($CH_3C(CH_3)CH_2OH$), and *tert*-butanol

($(CH_3)_3COH$). Butanol can be produced from biomass, which is then called biobutanol, and it can be considered as an alternative fuel with properties superior to those of ethanol.[237]

Although some work on the combustion of methanol and ethanol has been performed, detailed and systematic studies on the combustion chemistry of larger alcohols are largely lacking. A comprehensive experimental VUV PI-MBMS study of low-pressure premixed *n*- and *iso*-propanol flames has been reported by Li *et al.*[173] The identification of various flame species and the reported mole fraction profiles of lean and fuel-rich flames extend our current knowledge of the combustion chemistry of alcohols. However, the proposed formation pathways require validation by kinetic modeling studies. The effects of the fuel structure on the composition of butanol flames has been studied by Yang *et al.*[172] They employed single-photon VUV PI-MBMS to identify various intermediates in four different $\phi = 1.71$ flames fueled by one of the four butanol isomers. The authors described in detail the detection of various enols, including ethenol, propenols, and butenols. Special attention has been paid to the respective intermediate pool of the four flames, based on the chemical structure of the fuel. Their results show that the higher-mass oxygenated species are strongly affected by the fuel structure. However, several hydrocarbons have been found to be independent of the fuel structure.

Ethers: As a result of its high cetane number and low sooting characteristics, dimethyl ether (DME, CH_3OCH_3) has been proposed as a promising alternative diesel fuel and fuel additive for reducing particulate and NO_x emissions.[16, 238] The large-scale generation of DME via synthesis gas ($CO + H_2$) from non-petroleum based feedstocks, including coal, natural gas, and biomass, is presently explored as a promising alternative to conventional petroleum-derived fuels.[16] The composition of three different laminar low-pressure flames of DME have been studied with flame-sampling MBMS employing single-photon and electron ionization.[86,

239] Recent kinetic modeling has been essential to identify the key reaction pathways in the DME oxidation process;[21, 240-242] the DME combustion can be considered as very well understood. In Fig. 16(a) and (b) experimental and modeled mole fraction profiles of some key intermediates (CH_2O, C_2H_6, C_2H_4, C_2H_2, CH_4, CH_3, and HCO) are compared for a fuel-rich (ϕ = 1.20) low-pressure dimethyl ether flame.[239] A very good agreement between experimental data and kinetic model is observed. The results of the reaction path analysis are summarized schematically in Fig. 16(c). DME is mainly consumed through H-atom abstraction. The resulting CH_3OCH_2 subsequently decomposes by β-scission to form $CH_3 + CH_2O$ or reacts with O_2 to form $2CH_2O + OH$. Other pathways to formaldehyde are the reactions of $CH_3 + O$ to form $CH_2O + H$ and the dissociation of CH_3O. Formaldehyde is subsequently oxidized to CO_2 via HCO and CO. Methyl radicals, primarily formed through decomposition of CH_3OCH_2, recombine to form ethane, which generates ethyl radicals through subsequent reaction with H, OH, and O. Further hydrogen abstractions lead eventually to acetylene, which is oxidized further to yield CO.

Methyl *tert*-butyl ether ($CH_3OC(CH_3)_3$, MTBE) was one of the most frequently used oxygenate additives in gasoline, as it was used to enhance fuel octane.[243] Using an EI-MBMS study of three premixed MTBE flames at low pressures with equivalence ratios ranging from 0.18 to 1.84, van der Loos *et al.* [135] deduced the rate coefficients of H-atom abstraction from MTBE by highly reactive species like H, O, and OH. The use of flames burning at three different equivalence ratios facilitated the rate coefficients deduction: a lean MTBE-H_2-O_2 flame has been used to determine the rate coefficient of the reaction with O atoms, the rich flame is appropriate to deduce the rate coefficient of the reaction with H atoms, while the stoichiometric flame has been used to determine the rate coefficient expression of MTBE with OH. Furthermore, they

showed that almost all the MTBE conversion proceeds through isobutene formation, whereas the role of acetone remains negligible in the mechanism of MTBE oxidation in H_2-O_2 seeded flames. In a related study, Yao *et al.* [244] used VUV PI-MBMS to explore the influence of MTBE addition to laminar low-pressure gasoline-O_2 flames. However, the practical importance of MTBE combustion studies has become insignificant, as due to its toxicity to freshwater organisms,[245] MTBE is now mostly replaced by ethanol or DME.

Methyl And Ethyl Esters: Long-chain fatty acid methyl or ethyl esters are the main components of biodiesel, which is a renewable, increasingly important transportation fuel. The source of the fat or oil determines the nature of the hydrocarbon chain, while the alcohol used in the transesterification process dictates the type of ester.[10, 246] Experiments and modeling studies of real biodiesel are unfeasible as of today. Instead, the research focuses on short chain methyl and ethyl esters. Those molecules have relatively simple structures and are well-suited for combustion studies as they retain the functional ester group. The hydrocarbon backbone is expected to exhibit a similar chemistry to long-chain hydrocarbons.

Investigations of premixed laminar low-pressure flames of various biodiesel surrogates can explore the reaction pathways that account for fuel-specific differences in the production of aldehydes, ketones, CO, prompt CO_2, and the hydrocarbon precursors to PAH and soot. For example, the combustion chemistry of the isomeric fuels methylacetate (CH_3COOCH_3) and ethylformate ($HCOOC_2H_5$) has been studied by Oßwald *et al.* [247] employing VUV PI-MBMS. Comparison of identical flames of structural isomers allows detailed analysis of the influence of functional groups on the fuel consumption pathways. Differences in initial fuel destruction pathways are immediately visible, highlighting the influences of fuel structure on the combustion mechanisms.

Although the temperature profiles and mole fraction profiles for the major species (H_2, H_2O, CO, O_2, Ar, CO_2, fuels) were found to be quite similar in both flames, Oßwald *et al.* [247] pointed out differences in the intermediate species pools, some of which are summarized in Fig. 16. For example, the direct formation of C_2H_4 by H-abstraction of a primary hydrogen from the ethoxy group of ethylformate, followed by β-scission, was identified as a possible source for the enhancement of C_2 and C_4 species in the ethylformate flame – Fig. 17(a). Furthermore, the H-abstraction from the methoxy group of the methyl ester and from the ethoxy group of the ethyl ester lead preferentially to the formation of formaldehyde in the methylacetate flame and acetaldehyde in the ethylformate flame, respectively – Fig. 17(b). However, detailed modeling studies are needed to further assess the importance of different reactions pathways.

4. Conclusions and Outlook

Flame-sampling molecular-beam mass spectrometry of premixed laminar low-pressure flames allows for studies of combustion processes on a molecular level. The experimental approaches, e.g. flame geometry, sampling probe, ionization techniques and mass separation, have been described. Recent advances from the experimental aspect have been highlighted. For example, great progress has been made (a) in observing the effects of probe-induced perturbations and (b) employing tunable vacuum-ultraviolet synchrotron radiation for single-photon ionization. The first aspect permits a quantitative analysis of the flame data, while the latter aspect facilitates isomer-resolved measurements.

From the combustion chemistry perspective, recent flame studies have been focused on molecular-weight growth processes in hydrocarbon flames and reaction paths in flames of oxygenated, alternative fuels, like alcohols, ethers, and esters. Taking advantage of the tunability

of VUV synchrotron radiation, isomeric forms of several resonantly stabilized radicals, which are potentially important in aromatic ring formation processes, have been resolved. For example, triplet propargylene (^{3}HCCCH), *i*-C_4H_3, *i*-C_4H_5, CH_3CCCH_2 and/or CH_3CHCCH, *i*- and *n*-C_5H_3, and *l*- and *cyclic*-C_5H_5 have been unambiguously identified in a variety of different fuel-rich flames. Furthermore, isomer-specific measurements of C_3-C_7 closed-shell species have been summarized, including identification of various C_5H_x isomers, C_5H_5CCH and/or $C_5H_4CCH_2$ for the sum formula C_7H_6, and cycloheptatriene besides toluene at C_7H_8. Although the investigation of flames fueled by oxygenated species has just begun, the considerable advances which have been made so far, are described. For example, the combustion chemistry of ethanol and its isomer DME can be considered as very well understood. Experimental data exist for flames of larger molecules, including alcohols, ethers and esters, however, detailed chemical models for flames of those molecules are essential to follow their combustion chemistry.

Single-photon ionization by tunable VUV synchrotron radiation has been proven to be of particular importance in order to address combustion chemistry problems based on the isomeric nature of the reactants and products. However, access to beamtime at synchrotron user facilities is highly competitive and restricted. Maybe future laboratory-based laser light sources will be able to provide easily-tunable, high-resolution vacuum-ultraviolet radiation of suitable intensity for photoionization measurements. Furthermore, the energy resolution of the ionizing synchrotron photons will not be sufficient to resolve very similar isomers, whereas laser-based photoioinization typically can provide superior energy resolution. Another critical aspect from the experimental point of view is a more quantitative description of probe induced disturbances. The two-dimensional flow field created by the sampling probe should be included into the

modeling of those laminar premixed flames in order to ultimately develop more reliable combustion chemistry models.

In combination with constantly improving modeling capabilities, many outstanding problems in combustion chemistry can be unraveled by flame-sampling molecular-beam mass spectrometry. Future work is likely to include many more studies of hydrocarbon flames, with the focus being on larger, more structurally complex hydrocarbons that are present in liquid fuels. The flame chemistry of larger hydrocarbons can differ significantly from those of smaller molecules, especially in view of the production of precursors to aromatic species by unimolecular decomposition processes. Now that the formation of benzene can be considered as well understood, future research supposedly shifts towards the chemistry beyond the first aromatic ring in order to understand the formation of PAH's. In addition, the combustion chemistry of oxygenated compounds, e.g. alcohols, ethers, and esters will receive increasing interest, especially with respect to potential undesired emissions. These alternative non-petroleum based fuels will become more common in the future as replacements for or additives to conventional gasoline and diesel fuels. Also, not only oxygenated compounds can be abundant in biomass-derived fuels but also nitrogen-containing species. Therefore, advantage is likely to be taken of the increasing experimental capabilities in order to systematically study the combustion chemistry of N-containing fuel surrogates.

Acknowledgements:

Sandia is a multi-program laboratory operated by Sandia Corporation, a Lockheed Martin Company, for the National Nuclear Security Administration under contract DE-AC04-94-AL85000. PRW and TAC are supported by the Division of Chemical Sciences, Geosciences, and

Biosciences, the Office of Basic Energy Sciences, the U. S. Department of Energy, under grants DE-FG02-91ER14192 and DE-FG02-01ER15180, respectively, and by the Chemical Science Division of the U.S. Army Research Office (TAC). KKH is supported by the Deutsche Forschungsgemeinschaft under contract KO 1363/18-3.

References:

[1] Miller JA, Bowman CT. Mechanism and modeling of nitrogen chemistry in combustion. Prog Energy Combust Sci 1989;15:287-338.

[2] Richter H, Howard JB. Formation of polycyclic aromatic hydrocarbons and their growth to soot - a review of chemical reaction pathways. Prog Energy Combust Sci 2000;26:565-608.

[3] Boffetta P, Jourenkova N, Gustavsson P. Cancer risk from occupational and environmental exposure to polycyclic aromatic hydrocarbons. Cancer Cause Control 1997;8:444-72.

[4] Boström CE, Gerde P, Hanberg A, Jernström B, Johansson C, Kyrklund T, et al. Cancer risk assessment, indicators, and guidelines for polycyclic aromatic hydrocarbons in the ambient air. Environ Health Persp 2002;110:451-88.

[5] Miller JA, Pilling MJ, Troe J. Unravelling combustion mechanisms through a quantitative understanding of elementary reactions. Proc Combust Inst 2005;30:43-88.

[6] McEnally CS, Lisa DP, Burak A, Kohse-Höinghaus K. Studies of aromatic hydrocarbon formation mechanisms in flames: Progress towards closing the fuel gap. Prog Energy Combust Sci 2006;32:247-94.

[7] Agarwal AK. Biofuels (alcohols and biodiesel) applications as fuels for internal combustion engines. Prog Energy Combust Sci 2007;33:233-71.

[8] Demirbas A. Progress and recent trends in biofuels. Prog Energy Combust Sci 2007;33:1-18.

[9] Kheshgi HS, Prince RC, Marland G. The potential of biomass fuels in the context of global climate change: Focus on transportation fuels. Annu Rev Energy Environ 2000;25:199-244.

[10] Graboski MS, McCormick RL. Combustion of fat and vegetable oil derived fuels in diesel engines. Prog Energy Combust Sci 1998;24:125-64.

[11] Fisher EM, Pitz WJ, Curran HJ, Westbrook CK. Detailed chemical kinetic mechanisms for combustion of oxygenated fuels. Proc Combust Inst 2000;28:1579-86.

[12] Wu J, Song KH, Litzinger T, Lee SY, Santoro R, Linevsky M, et al. Reduction of PAH and soot in premixed ethylene-air flames by addition of ethanol. Combust Flame 2006;144:675-87.

[13] McNesby KL, Miziolek AW, Nguyen T, Delucia FC, Skaggs RR, Litzinger TA. Experimental and computational studies of oxidizer and fuel side addition of ethanol to opposed flow air/ethylene flames. Combust Flame 2005;142:413-27.

[14] Westbrook CK, Pitz WJ, Curran HJ. Chemical kinetic modeling study of the effects of oxygenated hydrocarbons on soot emisions from diesel engines. J Phys Chem A 2006;110:6912-22.

[15] Song KH, Nag P, Litzinger TA, Haworth DC. Effects of oxygenated additives on aromatic species in fuel-rich, premixed ethane combustion: A modeling study. Combust Flame 2003;135:341-49.

[16] Semelsberger TA, Borup RL, Greene HL. Dimethyl ether (DME) as an alternative fuel. J Power Sources 2006;156:497-511.

[17] Westbrook CK, Mizobuchi Y, Poinsot TJ, Smith PJ, Warnatz J. Computational combustion. Proc Combust Inst 2005;30:125-57.

[18] Lindstedt P. Modeling of the chemical complexities of flames. Proc Combust Inst 1998;27:269-85.

[19] Simmie JM. Detailed chemical kinetic models for the combustion of hydrocarbon fuels. Prog Energy Combust Sci 2003;29:599-634.

[20] Petrova MV, Williams FA. A small detailed chemical-kinetic mechanism for hydrocarbon combustion. Combust Flame 2006;144:526-44.

[21] Zhao Z, Chaos M, Kazakov A, Dryer FL. Thermal decomposition reaction and a comprehensive kinetic model of dimethyl ether. Int J Chem Kin 2008;40:1-18.

[22] Homann KH, Mochizuki M, Wagner HG. Über den Reaktionsablauf in fetten Kohlenwasserstoff-Sauerstoff-Flammen. Z Phys Chem NF 1963;37:299-313.

[23] Biordi JC. Molecular beam mass spectrometry for studying the fundamental chemistry of flames. Prog Energy Combust Sci 1977;3:151-73.

[24] Cool TA, Nakajima K, Mostefaoui TA, Qi F, McIlroy A, Westmoreland PR, et al. Selective detection of isomers with photoionization mass spectrometry for studies of hydrocarbon flame chemistry. J Chem Phys 2003;119:8356-65.

[25] Kohse-Höinghaus K, Barlow RS, Aldén M, Wolfrum J. Combustion at the focus: Laser diagnostics and control. Proc Combust Inst 2005;30:89-123.

[26] Mätzing H, Wagner HG. Measurements about the influence of pressure on carbon formation in premixed laminar C_2H_4-air flames. Proc Combust Inst 1988;21:1047-55.

[27] Kohse-Höinghaus K, Jeffries JB, editors, Applied combustion diagnostics. New York: Taylor & Francis, 2002.

[28] Eckbreth AC, Laser diagnostics for combustion temperature and species, Taylor & Francis, New York, 1996.

[29] Kohse-Höinghaus K. Laser techniques for the quantitative detection of reactive intermediates in combustion systems. Prog Energy Combust Sci 1994;20:203-79.

[30] Daily JW. Laser induced fluorescence spectroscopy in flames. Prog Energy Combust Sci 1997;23:133-99.

[31] Kohse-Höinghaus K, Jeffries JB, Copeland RA, Smith GP, Crosley DR. The quantitative LIF determination of OH concentrations in low-pressure flames. Proc Combust Inst 1988;22:1857-66.

[32] Rensberger KJ, Jeffries JB, Copeland RA, Kohse-Höinghaus K, Wise ML, Crosley DR. Laser-induced fluorescence determination of temperatures in low-pressure flames. Appl Opt 1989;28:3556-66.

[33] Luque J, Crosley DR. Radiative, collisional, and predissociative effects in CH laser-induced-fluorescence flame thermometry. Appl Opt 1999;38:1423-33.

[34] Tamura M, Luque J, Harrington JE, Berg PA, Smith GP, Jeffries JB, et al. Laser-induced fluorescence of seeded nitric oxide as a flame thermometer. Appl Phys B 1998;66:503-10.

[35] Hartlieb AT, Atakan B, Kohse-Höinghaus K. Temperature measurement in fuel-rich non-sooting low-pressure hydrocarbon flames. Appl Phys B 2000;70:435-45.

[36] Hartlieb AT, Atakan B, Kohse-Höinghaus K. Effects of a sampling quartz nozzle on the flame structure of a fuel-rich low-pressure propene flame. Combust Flame 2000;121:610-24.

[37] Heitor MV, Moreira ALN. Thermocouples and sample probes for combustion studies. Prog Energy Combust Sci 1993;19:259-78.

[38] Shaddix CR. Correcting thermocouple measurements for radiation loss: A critical review. Proc 33rd National Heat Transfer Conf 1999;1-10.

[39] Madson JM, Theby EA. SiO_2 coated thermocouples. Combust Sci Technol 1984;36:205-09.

[40] Burton KA, Ladouceur HD, Fleming JW. An improved noncatalytic coating for thermocouples. Combust Sci Technol 1992;81:141-45.

[41] Kent JH. Noncatalytic coating for platinum-rhodium thermocouples. Combust Flame 1970;14:279-81.

[42] Shandross RA, Longwell JP, Howard JB. Noncatalytic thermocouple coating for low-pressure flames. Combust Flame 1991;85:282-84.

[43] Kreiss K, Day GA, Schuler CR. Beryllium: A modern industrial hazard. Annu Rev Publ Health 2007;28:259-77.

[44] Bahlawane N, Struckmeier U, Kasper TS, Oßwald P. Noncatalytic thermocouple coatings produced with chemical vapor deposition for flame temperature measurements. Rev Sci Instr 2007;78:013905.

[45] Biordi JC, Lazzara CP, Papp JF. Molecular-beam mass-spectrometry applied to determining kinetics of reactions in flames. 1. Emperical characterization of flame perturbation by molecular-beam sampling probes. Combust Flame 1974;23:73-82.

[46] Knuth EL. Composition distortion in MBMS sampling. Combust Flame 1995;103:171-80.

[47] Seery DJ, Zabielski MF. Comparisons between flame species measured by probe sampling and optical spectrometry techniques. Combust Flame 1989;78:169-77.

[48] Stepowski D, Puechberty D, Cottereau MJ. Use of laser-induced fluorescence of OH to study the perturbation of a flame by a probe. Proc Combust Inst 1981;18:1567-73.

[49] Smith OI, Chandler DW. An experimental study of probe distortions to the structure of one-dimensional flames. Combust Flame 1986;63:19-29.

[50] Pauwels JF, Carlier M, Devolder P, Sochet LR. Experimental and numerical analysis of a low pressure stoichiometric methanol-air flame. Combust Sci Technol 1989;64:97-117.

[51] Desgroux P, Gasnot L, Pauwels JF, Sochet LR. Correction of LIF temperature measurements for laser absorption and fluorescence trapping in a flame: Application to the thermal perturbation study induced by a sampling probe. Appl Phys B 1995;61:401-07.

[52] Bastin E, Delfau JL, Reuillon M, Vovelle C. Experimental and computational investigation of the structure of a sooting C_2H_2-O_2-Ar flame. Proc Combust Inst 1988;22:313-22.

[53] Westmoreland PR, Law ME, Cool TA, Wang J, McIlroy A, Taatjes CA, et al. Analysis of flame structure by molecular-beam mass spectrometry using electron-impact and synchrotron-photon ionization. Combust Expl Shock Waves 2006;42:672-77.

[54] Bittner JD, Howard JB. Composition profiles and reaction mechanisms in a near-sooting premixed benzene/oxygen/argon flame. Proc Combust Inst 1981;18:1105-16.

[55] Bhargava A, Westmoreland PR. MBMS analysis of a fuel-lean ethylene flame. Combust Flame 1998;115:456-67.

[56] Hayhurst AN, Kittelson DB, Telford NR. Mass spectrometric sampling of ions from atmospheric pressure flames - II: Aerodynamic disturbance of a flame by the sampling systems. Combust Flame 1977;28:123-35.

[57] Yi AC, Knuth EL. Probe-induced concentration distortions in molecular-beam mass-spectrometer sampling. Combust Flame 1986;63:369-79.

[58] Cattolica RJ, Yoon S, Knuth EL. OH concentration in an atmospheric-pressure methane-air flame from molecular-beam mass spectrometry and laser-absorption spectroscopy. Combust Sci Technol 1982;28:225-39.

[59] Kamphus M, Liu NN, Atakan B, Qi F, McIlroy A. REMPI temperature measurement in molecular beam sampled low-pressure flames. Proc Combust Inst 2003;29:2627-33.

[60] Dempster AJ. A new method of positive ray analysis. Phys Rev 1918;11:316-25.

[61] Nier AO. A mass spectrometer for isotope and gas analysis. Rev Sci Instr 1947;18:398-411.

[62] Mirsaleh-Kohan N, Robertson WD, Compton RN. Electron ionization time-of-flight mass spectrometry: Historical review and current applications. Mass Spectrom Rev 2008;27:237-85.

[63] Ledingham KWD, Singhal RP. High intensity laser mass spectrometry - a review. Int J Mass Spectrom Ion Proc 1997;163:149-68.

[64] Lockyer NP, Vickerman JC. Single photon ionisation mass spectrometry using laser-generated vacuum ultraviolet photons. Laser Chem 1997;17:139-59.

[65] Homann KH, Wagner HG. Untersuchung des Reaktionsablaufs in fetten Kohlenwasserstof-Sauerstoff-Flammen. 2. Versuche an rußenden Acetylen-Sauerstoff-Flammen bei niedrigem Druck. Ber Bunsenges Phys Chem 1965;69:20.

[66] Peeters J, Mahnen G. Reaction mechanisms and rate constants of elementary steps in methane-oxygen flames. Proc Combust Inst 1973;14:133-46.

[67] Vandooren J, Branch MC, van Tiggelen PJ. Comparisons of the structure of stoichiometric CH_4-N_2O-Ar and CH_4-O_2-Ar flames by molecular beam sampling and mass spectrometric analysis. Combust Flame 1992;90:247-58.

[68] Böhm H, Lamprecht A, Atakan B, Kohse-Höinghaus K. Modelling of a fuel-rich premixed propene-oxygen-argon flame and comparison with experiments. Phys Chem Chem Phys 2000;2:4956-61.

[69] Bonne U, Homann KH, Wagner HG. Carbon formation in premixed flames. Proc Combust Inst 1965;10:503-12.

[70] Ahrens J, Bachmann M, Baum T, Griesheimer J, Kovacs R, Weilmünster P, et al. Fullerenes and their ions in hydrocarbon flames. Int J Mass Spectrom Ion Proc 1994;138:133-48.

[71] Ahrens J, Keller A, Kovacs R, Homann KH. Large molecules, radicals, ions, and small soot particles in fuel-rich hydrocarbon flames - Part III: REMPI mass spectrometry of large flame PAHs and fullerenes and their quantitative calibration through sublimation. Ber Bunsenges Phys Chem 1998;102:1823-39.

[72] Ahrens J, Kovacs R, Shafranovskii EA, Homann KH. Online multiphoton ionization mass-spectrometry applied to PAH and fullerenes in flames. Ber Bunsenges Phys Chem 1994;98:265-68.

[73] Homann KH. Fullerenes and soot formation - new pathways to large particles in flames. Angew Chem Int Ed 1998;37:2435-51.

[74] Kamphus M, Braun-Unkhoff M, Kohse-Höinghaus K. Formation of small PAHs in laminar premixed low-pressure propene and cyclopentene flames: Experiment and modeling. Combust Flame 2008;152:28-59.

[75] Kasper TS, Oßwald P, Kamphus M, Kohse-Höinghaus K. Ethanol flame structure investigated by molecular beam mass spectrometry. Combust Flame 2007;150:220-31.

[76] Keller A, Kovacs R, Homann KH. Large molecules, ions, radicals and small soot particles in fuel-rich hydrocarbon flames. Part IV. Large polycyclic aromatic hydrocarbons and their radicals in a fuel-rich benzene-oxygen flame. Phys Chem Chem Phys 2000;2:1667-75.

[77] Kohse-Höinghaus K, Atakan B, Lamprecht A, González Alatorre G, Kamphus M, Kasper T, et al. Contributions to the investigation of reaction pathways in fuel-rich flames. Phys Chem Chem Phys 2002;4:2056-62.

[78] Kohse-Höinghaus K, Schocker A, Kasper T, Kamphus M, Brockhinke A. Combination of laser- and mass-spectroscopic techniques for the investigation of fuel-rich flames. Z Phys Chem 2005;219:583-99.

[79] Meier U, Kohse-Höinghaus K. REMPI detection of CH_3 in low-pressure flames. Chem Phys Lett 1987;142:498-502.

[80] Marangos JP, Shen N, Ma H, Hutchinson MHR, Connerade JP. Broadly tunable vacuum-ultraviolet radiation source employing resonant enhanced sum-difference frequency mixing in krypton. J Opt Soc Am B 1990;7:1254-9.

[81] Yamanouchi K. Tunable vacuum ultraviolet laser - ideal light for spectroscopy of atoms, molecules, and clusters. J Electron Spectrosc 1996;80:267-70.

[82] Yamanouchi K, Tsuchiya S. Tunable vacuum ultraviolet laser spectroscopy: Excited state dynamics of jet-cooled molecules and van der Waals complexes. J Phys B 1995;28:133-65.

[83] Kung AH, Young JF, Harris SE. Generation of 1182-Å radiation in phase-matched mixtures of inert gases. Appl Phys Lett 1973;22:301-02.

[84] Hilbig R, Wallenstein R. Enhanced production of tunable VUV radiation by phase-matched frequency tripling in Krypton and Xenon. IEEE J Quant Electr 1981;17:1566-73.

[85] Ng CY. Vacuum ultraviolet spectroscopy and chemistry by photoionization and photoelectron methods. Annu Rev Phys Chem 2002;53:101-40.

[86] McIlroy A, Hain TD, Michelsen HA, Cool TA. A laser and molecular beam mass spectrometer study of low-pressure dimethyl ether flames. Proc Combust Inst 2000;28:1647-53.

[87] Qi F, McIlroy A. Identifying combustion intermediates via tunable vacuum ultraviolet photoionization mass spectrometry. Combust Sci Technol 2005;177:2021-37.

[88] Werner JH, Cool TA. Flame sampling photoionization mass spectrometry of CH_3PO_2 and CH_3OPO_2. Chem Phys Lett 1997;275:278-82.

[89] Werner JH, Cool TA. Flame sampling photoionization mass spectrometry of dichloroethenol. Chem Phys Lett 1998;290:81-87.

[90] Werner JH, Cool TA. Kinetic model for the decomposition of DMMP in a hydrogen/oxygen Flame. Combust Flame 1999;117:78-98.

[91] Werner JH, Cool TA. The kinetics of the combustion of trichloroethylene for low C/H ratios. Combust Flame 2000;120:125-42.

[92] Bermudez G, Pfefferle LD. Laser ionization time-of-flight mass spectrometry combined with residual gas analysis for the investigation of moderate temperature benzene oxidation. Combust Flame 1995;100:41-51.

[93] McEnally CS, Pfefferle LD, Mohammed RK, Smooke MD, Colket MB. Mapping of trace hydrocarbon concentrations in two-dimensional flames using single-photon photoionization mass spectrometry. Anal Chem 1999;71:364-72.

[94] Happold J, Grotheer HH, Aigner M. Distinction of gaseous soot precursor molecules and soot precursor particles through photoionization mass spectrometry. Rapid Commun Mass Spectrom 2007;21:1247-54.

[95] Cool TA, McIlroy A, Qi F, Westmoreland PR, Poisson L, Peterka DS, et al. Photoionization mass spectrometer for studies of flame chemistry with a synchrotron light source. Rev Sci Instr 2005;76:094102.

[96] Yang R, Wang J, Huang C, Yang B, Wei L, Shan X, et al. Combustion study with synchrotron radiation single-photon ionization technique. Chin Sci Bull 2005;50:1082-86.

[97] Paul W, Steinwedel H. Ein neues Massenspektrometer ohne Magnetfeld. Z Naturforsch A 1953;8:448-50.

[98] Stephens WE. A pulsed mass spectrometer with time dispersion. Phys Rev 1946;69:691.

[99] Wiley WC, McLaren IH. Time-of-flight mass spectrometer with improved resolution. Rev Sci Instr 1955;26:1150-57.

[100] Weickhardt C, Moritz F, Grotemeyer J. Time-of-flight mass spectrometry: State-of-the-art in chemical analysis and molecular science. Mass Spectrom Rev 1996;15:139-62.

[101] Guilhaus M. Principles and instrumentation in time-of-flight mass-spectrometry - physical and instrumental concepts. J Mass Spectrom 1995;30:1519-32.

[102] Mamyrin BA. Laser assisted reflectron time-of-flight mass-spectrometry. Int J Mass Spectrom Ion Proc 1994;131:1-19.

[103] Mamyrin BA. Time-of-flight mass spectrometry (concepts, achievements, and prospects). Int J Mass Spectrom 2001;206:251-66.

[104] Hansen N, Kasper T, Klippenstein SJ, Westmoreland PR, Law ME, Taatjes CA, et al. Initial steps of aromatic ring formation in a laminar premixed fuel-rich cyclopentene flame. J Phys Chem A 2007;111:4081-92.

[105] Cool TA, Nakajima K, Taatjes CA, McIlroy A, Westmoreland PR, Law ME, et al. Studies of a fuel-rich propane flame with photoionization mass spectrometry. Proc Combust Inst 2005;30:1681-88.

[106] Duric N, Cadez I, Kurepa M. Electron impact total ionization cross-sections for methane, ethane and propane. Int J Mass Spectrom Ion Proc 1991;108:R1-R10.

[107] Nishimura H, Tawara H. Total electron impact ionization cross sections for simple hydrocarbon molecules. J Phys B 1994;27:2063-74.

[108] Cool TA, Wang J, Nakajima K, Taatjes CA, McIlroy A. Photoionization cross sections for reaction intermediates in hydrocarbon combustion. Int J Mass Spectrom 2005;247:18-27.

[109] Wang J, Yang B, Cool TA, Hansen N, Kasper T. Near-threshold absolute photoionization cross-sections of some reaction intermediates in combustion. Int J Mass Spectrom 2008;269:210-20.

[110] Robinson JC, Sveum NE, Neumark DM. Determination of absolute photoionization cross sections for vinyl and propargyl radicals. J Chem Phys 2003;119:5311-14.

[111] Robinson JC, Sveum NE, Neumark DM. Determination of absolute photoionization cross sections for isomers of C_3H_5: Allyl and 2-propenyl radicals. Chem Phys Lett 2004;383:601-05.

[112] Sveum NE, Goncher SJ, Neumark DM. Determination of absolute photoionization cross sections of the phenyl radical. Phys Chem Chem Phys 2006;8:592-98.

[113] Otvos JW, Stevenson DP. Cross-sections of molecules for ionization by electrons. J Am Chem Soc 1956;78:546-51.

[114] Fitch WL, Sauter AD. Calculation of relative electron impact total ionization cross sections for organic molecules. Anal Chem. 1983;55:832-35.

[115] Becker KH, Tarnovsky V. Electron-impact ionization of atoms, molecules, ions and transient species. Plasma Sources Sci Technol 1995;4:307-15.

[116] Deutsch H, Becker K, Matt S, Märk TD. Theoretical determination of absolute electron-impact ionization cross sections of molecules. Int J Mass Spectrom 2000;197:37-69.

[117] Probst M, Deutsch H, Becker K, Märk TD. Calculations of absolute electron-impact ionization cross sections for molecules of technological relevance using the DM formalism. Int J Mass Spectrom 2001;206:13-25.

[118] Hwang W, Kim YK, Rudd ME. New model for electron-impact ionization cross sections of molecules. J Chem Phys 1996;104:2956-66.

[119] Koizumi H. Predominant decay channel for superexcited organic molecules. J Chem Phys 1991;95:5846-52.

[120] Bobeldijk M, van der Zande WJ, Kistemaker PG. Simple models for the calculation of photoionization and electron impact ionization cross sections of polyatomic molecules. Chem Phys 1994;179:125-30.

[121] Heimann PA, Koike M, Hsu CW, Blank D, Yang XM, Suits AG, et al. Performance of the vacuum ultraviolet high-resolution and high-flux beamline for chemical dynamics studies at the Advanced Light Source. Rev Sci Instr 1997;68:1945-51.

[122] Suits AG, Heimann P, Yang X, Evans M, Hsu CW, Lu KT, et al. A differentially pumped harmonic filter on the chemical-dynamics beamline at the Advanced Light Source. Rev Sci Instr 1995;66:4841-44.

[123] Qi F, Yang R, Yang B, Huang C, Wei L, Wang J, et al. Isomeric identification of polycyclic aromatic hydrocarbons formed in combustion with tunable vacuum ultraviolet photoionization. Rev Sci Instr 2006;77:084101.

[124] Huang C, Yang B, Yang R, Wang J, Wei L, Shan X, et al. Modification of photoionization mass spectrometer with synchrotron radiation as ionization source. Rev Sci Instr 2005;76:126108.

[125] Taatjes CA, Hansen N, McIlroy A, Miller JA, Senosiain JP, Klippenstein SJ, et al. Enols are common intermediates in hydrocarbon oxidation. Science 2005;308:1887-89.

[126] Taatjes CA, Hansen N, Miller JA, Cool TA, Wang J, Westmoreland PR, et al. Combustion chemistry of enols: Possible ethenol precursors in flames. J Phys Chem A 2006;110:3254-60.

[127] Taatjes CA, Hansen N, Osborn DL, Kohse-Höinghaus K, Cool TA, Westmoreland PR. "Imaging" combustion chemistry via multiplexed synchrotron-photoionization mass spectrometry. Phys Chem Chem Phys 2008;10:20-34.

[128] Hansen N, Klippenstein SJ, Miller JA, Wang J, Cool TA, Law ME, et al. Identification of C_5H_x isomers in fuel-rich flames by photoionization mass spectrometry and electronic structure calculations. J Phys Chem A 2006;110:4376-88.

[129] Taatjes CA, Osborn DL, Cool TA, Nakajima K. Synchrotron photoionization measurements of combustion intermediates: The photoionization efficiency of HONO. Chem Phys Lett 2004;394:19-24.

[130] Bhargava A, Westmoreland PR. Measured flame structure and kinetics in a fuel-rich ethylene flame. Combust Flame 1998;113:333-47.

[131] Vandooren J, Oldenhove de Guertechin L, van Tiggelen PJ. Kinetics in a lean formaldehyde flame. Combust Flame 1986;64:127-39.

[132] Musick M, van Tiggelen PJ, Vandooren J. Experimental study of the structure of several fuel-rich premixed flames of methane, oxygen, and argon. Combust Flame 1996;105:433-50.

[133] Ancia R, van Tiggelen PJ, Vandooren J. Experimental investigation in rich premixed acetylene flames. Exp Therm Fluid Sci 2004;28:715-22.

[134] Ancia R, Vandooren J, van Tiggelen PJ. Experimental study of the structure of rich ethane flames. Proc Combust Inst 1996;26:1009-16.

[135] van der Loos A, Vandooren J, van Tiggelen PJ. Kinetic study of methyl *tert*-butyl ether (MTBE) oxidation in flames. Proc Combust Inst 1998;27:477-84.

[136] Miller JA, Melius CF. Kinetic and thermodynamic issues in the formation of aromatic compounds in flames of aliphatic fuels. Combust Flame 1992;91:21-39.

[137] Miller JA, Klippenstein SJ. The recombination of propargyl radicals and other reactions on a C_6H_6 potential. J Phys Chem A 2003;107:7783-99.

[138] Pope CJ, Miller JA. Exploring old and new benzene formation pathways in low-pressure premixed flames of aliphatic fuels. Proc Combust Inst 2000;28:1519-27.

[139] Marinov NM, Castaldi MJ, Melius CF, Tsang W. Aromatic and polycyclic aromatic hydrocarbon formation in a premixed propane flame. Combust Sci Technol 1997;128:295-342.

[140] Mebel AM, Jackson WM, Chang AHH, Lin SH. Photodissociation dynamics of propyne and allene: A view from *ab initio* calculations of the C_3H_n (n = 1-4) species and the isomerization mechanism for C_3H_2. J Am Chem Soc 1998;120:5751-63.

[141] Rubio M, Stalring J, Bernhardsson A, Lindh R, Roos BO. Theoretical studies of isomers of C_3H_2 using a multiconfigurational approach. Theor Chem Acc 2000;105:15-30.

[142] Taatjes CA, Klippenstein SJ, Hansen N, Miller JA, Cool TA, Wang J, et al. Synchrotron photoionization measurements of combustion intermediates: Photoionization efficiency and identification of C_3H_2 isomers. Phys Chem Chem Phys 2005;7:806-13.

[143] Miller JA, Volponi JV, Pauwels JF. The effect of allene addition on the structure of a rich $C_2H_2/O_2/Ar$ flame. Combust Flame 1996;105:451-61.

[144] Miller JA, Klippenstein SJ. From the multiple-well master equation to phenomenological rate coefficients: Reactions on a C_3H_4 potential energy surface. J Phys Chem A 2003;107:2680-92.

[145] Hansen N, Klippenstein SJ, Taatjes CA, Miller JA, Wang J, Cool TA, et al. Identification and chemistry of C_4H_3 and C_4H_5 isomers in fuel-rich flames. J Phys Chem A 2006;110:3670-78.

[146] Domin D, Lester WA, Whitesides R, Frenklach M. Isomer energy differences for the C_4H_3 and C_4H_5 isomers using diffusion Monte Carlo. J Phys Chem A 2008;112:2065-68.

[147] Wheeler SE, Allen WD, Schaefer HF. Thermochemistry of disputed soot formation intermediates C_4H_3 and C_4H_5. J Chem Phys 2004;121:8800-13.

[148] Wang H, Frenklach M. A detailed kinetic modeling study of aromatics formation in laminar premixed acetylene and ethylene flames. Combust Flame 1997;110:173-221.

[149] Wang H, Frenklach M. Calculations of rate coefficients for the chemically activated reactions of acetylene with vinylic and aromatic radicals. J Phys Chem 1994;98:11465-89.

[150] Cole JA, Bittner JD, Longwell JP, Howard JB. Formation mechanisms of aromatic compounds in aliphatic flames. Combust Flame 1984;56:51-70.

[151] Frenklach M, Clary DW, Gardiner WC, Stein SE. Detailed kinetic modeling of soot formation in shock-tube pyrolysis of acetylene. Proc Combust Inst 1985;20:887-901.

[152] Frenklach M, Warnatz J. Detailed modeling of PAH profiles in a sooting low-pressure acetylene flame. Combust Sci Technol 1987;51:265-83.

[153] Westmoreland PR, Dean AM, Howard JB, Longwell JP. Forming benzene in flames by chemically activated isomerization. J Phys Chem 1989;93:8171-80.

[154] Senosiain JP, Miller JA. The reaction of *n*- and *i*-C_4H_5 radicals with acetylene. J Phys Chem A 2007;111:3740-47.

[155] Walch SP. Characterization of the minimum energy paths for the ring closure reactions of C_4H_3 with acetylene. J Chem Phys 1995;103:8544-47.

[156] Klippenstein SJ, Miller JA. The addition of hydrogen atoms to diacetylene and the heats of formation of *i*-C_4H_3 and *n*-C_4H_3. J Phys Chem A 2005;109:4285-95.

[157] Melius CF, Colvin ME, Marinov NM, Pitz WJ, Senkan SM. Reaction mechanisms in aromatic hydrocarbon formation involving the C_5H_5 cyclopentadienyl moiety. Proc Combust Inst 1996;26:685-92.

[158] Miller JA. Theory and modeling in combustion chemistry. Proc Combust Inst 1996;26:461-80.

[159] Yang B, Huang C, Wei L, Wang J, Sheng L, Zhang Y, et al. Identification of isomeric C_5H_3 and C_5H_5 free radicals in flame with tunable synchrotron photoionization. Chem Phys Lett 2006;423:321-26.

[160] Lindstedt P, Maurice L, Meyer M. Thermodynamic and kinetic issues in the formation and oxidation of aromatic species. Faraday Discuss 2001;119:409-32.

[161] Ikeda E, Tranter RS, Kiefer JH, Kern RD, Singh HJ, Zhang Q. The pyrolysis of methylcyclopentadiene: Isomerization and formation of aromatics. Proc Combust Inst 2000;28:1725-32.

[162] Moskaleva LV, Mebel AM, Lin MC. The CH_3+C_5H_5 reaction: A potential source of benzene at high temperatures. Proc Combust Inst 1996;26:521-26.

[163] Mebel AM, Lin SH, Yang XM, Lee YT. Theoretical study on the mechanism of the dissociation of benzene: The C_5H_3+CH_3 product channel. J Phys Chem A 1997;101:6781-89.

[164] Yang B, Li Y, Wei L, Huang C, Wang J, Tian Z, et al. An experimental study of the premixed benzene/oxygen/argon flame with tunable synchrotron photoionization. Proc Combust Inst 2007;31:555-63.

[165] Zhang Q, Li Y, Tian Z, Zhang T, Wang J, Qi F. Experimental study of premixed stoichiometric ethylene/oxygen/argon flame. Chin J Chem Phys 2006;19:379-85.

[166] Hansen N, Miller JA, Taatjes CA, Wang J, Cool TA, Law ME, et al. Photoionization mass spectrometric studies and modeling of fuel-rich allene and propyne flames. Proc Combust Inst 2007;31:1157-64.

[167] Goulay F, Osborn DL, Taatjes CA, Zou P, Meloni G, Leone SR. Direct detection of polyynes formation from the reaction of ethynyl radical (C_2H) with propyne (CH_3CCH) and allene (CH_2CCH_2). Phys Chem Chem Phys 2007;9:4291-300.

[168] Stahl F, Schleyer PV, Schaefer HF, Kaiser RI. Reactions of ethynyl radicals as a source of C_4 and C_5 hydrocarbons in Titan's atmosphere. Planet Space Sci 2002;50:685-92.

[169] Hansen N, Klippenstein SJ, Westmoreland PR, Kasper T, Kohse-Höinghaus K, Wang J, et al. A combined ab initio and photoionization mass spectrometric study of polyynes in fuel-rich flames. Phys Chem Chem Phys 2008;10:366-74.

[170] Huang C, Wei L, Yang B, Wang J, Li Y, Sheng L, et al. Lean premixed gasoline/oxygen flame studied with tunable synchrotron vacuum UV photoionization. Energy Fuels 2006;20:1505-13.

[171] Li Y, Huang C, Wei L, Yang B, Wang J, Tian Z, et al. An experimental study of rich premixed gasoline/O_2/Ar flame with tunable synchrotron vacuum ultraviolet photoionization. Energy Fuels 2007;21:1931-41.

[172] Yang B, Oßwald P, Li Y, Wang J, Wei L, Tian Z, et al. Identification of combustion intermediates in isomeric fuel-rich premixed butanol-oxygen flames at low pressure. Combust Flame 2007;148:198-209.

[173] Li Y, Wei L, Tian Z, Yang B, Wang J, Zhang T, et al. A comprehensive experimental study of low-pressure premixed C_3-oxygenated hydrocarbon flames with tunable synchrotron photoionization. Combust Flame 2008;152:336-59.

[174] Law ME, Carriére T, Westmoreland PR. Allene addition to a fuel-lean ethylene flat flame. Proc Combust Inst 2005;30:1353-61.

[175] Fascella S, Cavallotti C, Rota R, Carrà S. The peculiar kinetics of the reaction between acetylene and the cyclopentadienyl radical. J Phys Chem A 2005;109:7546-57.

[176] Cavallotti C, Mancarella S, Rota R, Carrà S. Conversion of C_5 into C_6 cyclic species through the formation of C_7 intermediates. J Phys Chem A 2007;111:3959-69.

[177] Marinov NM, Pitz WJ, Westbrook CK, Lutz AE, Vincitore AM, Senkan SM. Chemical kinetic modeling of a methane opposed-flow diffusion flame and comparison to experiments. Proc Combust Inst 1998;27:605-13.

[178] Langley CJ, Burgess AR. A study of premixed fuel-rich methane flames by molecular beam mass spectrometry: The primary reaction zone. Proc R Soc Lond A 1989;421:259-78.

[179] Peeters J, Vinckier C. Production of chemi-ions and formation of CH and CH_2 radicals in methane-oxygen and ethylene-oxygen flames. Proc Combust Inst 1975;15:969-77.

[180] Burgess AR, Langley CJ. The chemical structure of premixed fuel-rich methane flames: The effect of hydrocarbon species in the secondary reaction zone. Proc R Soc Lond A 1991;433:1-21.

[181] Hennessy RJ, Robinson C, Smith DB. A comparative study of methane and ethane flame chemistry by experiment and detailed modelling. Proc Combust Inst 1986;21:761-72.

[182] Crunelle B, Surdyk D, Pauwels JF, Sochet LR. Experimental Study of low-pressure premixed methane and ethane flames by molecular beam sampling and mass spectrometry analysis. J Chim Phys 1997;94:433-59.

[183] Crunelle B, Pauwels JF, Sochet LR. Kinetics of low pressure premixed $CH_4/O_2/Ar$ and $C_2H_6/O_2/Ar$ Flames. Bull Soc Chim Belg 1996;105:491-99.

[184] Lamprecht A, Atakan B, Kohse-Höinghaus K. Fuel-rich propene and acetylene flames: A comparison of their flame chemistries. Combust Flame 2000;122:483-91.

[185] Delfau JL, Vovelle C. Analyse par spectrométrie de masse de flammes C_2H_2/O_2 produisant des suies. J Chim Phys 1985;82:747-54.

[186] Musick M, van Tiggelen PJ, Vandooren J. Flame structure studies of several premixed ethylene-oxygen-argon flames at equivalence ratios from 1.00 to 2.00. Combust Sci Technol 2000;153:247-61.

[187] Carriere T, Westmoreland PR, Kazakov A, Stein YS, Dryer FL. Modeling ethylene combustion from low to high pressure. Proc Combust Inst 2003;29:1257-66.

[188] Douté C, Delfau JL, Vovelle C. Reaction mechanism for aromatics formation in a low pressure, premixed acetylene-oxygene/argon flame. Combust Sci Technol 1994;103:153-73.

[189] Atakan B, Hartlieb AT, Brand J, Kohse-Höinghaus K. An experimental investigation of premixed fuel-rich low-pressure propene/oxygen/argon flames by laser spectroscopy and molecular-beam mass spectrometry. Proc Combust Inst 1998;27:435-44.

[190] Richter H, Howard JB. Formation and consumption of single-ring aromatic hydrocarbons and their precursors in premixed acetylene, ethylene and benzene flames. Phys Chem Chem Phys 2002;4:2038-55.

[191] Westmoreland PR, Howard JB, Longwell JP. Tests of published mechanisms by comparison with measured laminar flame structure in fuel-rich acetylene combustion. Proc Combust Inst 1986;21:773-82.

[192] Rasmussen CL, Skjoth-Rasmussen MS, Jensen AD, Glarborg P. Propargyl recombination: Estimation of the high temperature, low pressure rate constant from flame measurements. Proc Combust Inst 2005;30:1023-31.

[193] Delfau JL, Vovelle C. Mechanism of soot formation in premixed C_2H_2/O_2 flames. Combust Sci Technol 1984;41:1-15.

[194] Davis SG, Law CK, Wang H. Propyne pyrolysis in a flow reactor: An experimental, RRKM, and detailed kinetic modeling study. J Phys Chem A 1999;103:5889-99.

[195] Lindstedt RP, Skevis G. Benzene formation chemistry in premixed 1,3-butadiene flames. Proc Combust Inst 1996;26:703-09.

[196] Hansen N, Miller JA, Kasper T, Kohse-Höinghaus K, Westmoreland PR, Wang J, et al. Benzene formation in premixed fuel-rich 1,3-butadiene flames. Proc Combust Inst 2008;accepted:

[197] González Alatorre G, Böhm H, Atakan B, Kohse-Höinghaus K. Experimental and modelling study of 1-pentene combustion at fuel-rich conditions. Z Phys Chem 2001;215:981-95.

[198] Marinov NM, Pitz WJ, Westbrook CK, Vincitore AM, Castaldi MJ, Senkan SM, et al. Aromatic and polycyclic aromatic hydrocarbon formation in a laminar premixed *n*-butane flame. Combust Flame 1998;114:192-213.

[199] Lamprecht A, Atakan B, Kohse-Höinghaus K. Fuel-rich flame chemistry in low-pressure cyclopentene flames. Proc Combust Inst 2000;28:1817-24.

[200] Lindstedt RP, Rizos KA. The formation and oxidation of aromatics in cyclopentene and methyl-cyclopentadiene mixtures. Proc Combust Inst 2002;29:2291-98.

[201] Atakan B, Lamprecht A, Kohse-Höinghaus K. An experimental study of fuel-rich 1,3-pentadiene and acetylene/propene flames. Combust Flame 2003;133:431-40.

[202] Law ME, Westmoreland PR, Cool TA, Wang J, Hansen N, Taatjes CA, et al. Benzene precursors and formation routes in a stoichiometric cyclohexane flame. Proc Combust Inst 2007;31:565-73.

[203] Zhang HR, Eddings EG, Sarofim AF. Combustion reactions of paraffin components in liquid transportation fuels using generic rates. Combust Sci Technol 2007;179:61-89.

[204] Zhang HR, Huynh LK, Kungwan N, Yang Z, Zhang S. Combustion modeling and kinetic rate calculations for a stoichiometric cyclohexane flame. 1. Major reaction pathways. J Phys Chem A 2007;111:4102-15.

[205] Silke EJ, Pitz WJ, Westbrook CK, Ribaucour M. Detailed chemical kinetic modeling of cyclohexane oxidation. J Phys Chem A 2007;111:3761-75.

[206] Bachmann M, Griesheimer J, Homann KH. The formation of C_{60} and its precursors in naphthalene flames. Chem Phys Lett 1994;223:506-10.

[207] Griesheimer J, Homann KH. Large molecules, radicals ions, and small soot particles in fuel-rich hydrocarbon flames. Part II. Aromatic radicals and intermediate PAHs in a premixed low-pressure naphthalene/oxygen/argon flame. Proc Combust Inst 1998;27:1753-59.

[208] Frenklach M. Reaction mechanism of soot formation in flames. Phys Chem Chem Phys 2002;4:2028-37.

[209] Lindstedt RP, Skevis G. Detailed kinetic modeling of premixed benzene flames. Combust Flame 1994;99:551-61.

[210] Zhang HY, McKinnon JT. Elementary reaction modeling of high-temperature benzene combustion. Combust Sci Technol 1995;107:261-300.

[211] Tan Y, Frank P. A detailed comprehensive kinetic model for benzene oxidation using the recent kinetic results. Proc Combust Inst 1996;26:677-84.

[212] Richter H, Grieco WJ, Howard JB. Formation mechanism of polycyclic aromatic hydrocarbons and fullerenes in premixed benzene flames. Combust Flame 1999;119:1-22.

[213] Richter H, Benish TG, Mazyar OA, Green WH, Howard JB. Formation of polycyclic aromatic hydrocarbons and their radicals in a nearly sooting premixed benzene flame. Proc Combust Inst 2000;28:2609-18.

[214] Ristori A, Dagaut P, El Bakali A, Pengloan G, Cathonnet M. Benzene oxidation: Experimental results in a JDR and comprehensive kinetic modeling in JSR, shock-tube and flame. Combust Sci Technol 2001;167:223-56.

[215] Defoeux F, Dias V, Renard C, van Tiggelen PJ, Vandooren J. Experimental investigation of the structure of a sooting premixed benzene/oxygen/argon flame burning at low pressure. Proc Combust Inst 2005;30:1407-15.

[216] Grieco WJ, Lafleur AL, Swallow KC, Richter H, Taghizadeh K, Howard JB. Fullerenes and PAH in low-pressure premixed benzene/oxygen flames. Proc Combust Inst 1998;27:1669-75.

[217] Richter H, Granata S, Green WH, Howard JB. Detailed modeling of PAH and soot formation in a laminar premixed benzene/oxygen/argon low-pressure flame. Proc Combust Inst 2005;30:1397-405.

[218] Bachmann M, Wiese W, Homann KH. PAH and aromeres: Precursors of fullerenes and soot. Proc Combust Inst 1996;26:2259-67.

[219] Homann KH. Formation of large molecules, particulates and ions in premixed hydrocarbon flames; progress and unresolved questions. Proc Combust Inst 1984;20:857-70.

[220] Wang J, Yang B, Li Y, Tian Z, Zhang T, Qi F, et al. The tunable VUV single-photon ionization mass spectrometry for the analysis of individual components in gasoline. Int J Mass Spectrom 2007;263:30-37.

[221] Pauwels JF, Carlier M, Sochet LR. Analysis by gas-phase electron spin resonance of H, O, OH, and halogen atoms in flames. J Phys Chem 1982;86:4330-35.

[222] Pauwels JF, Carlier M, Devolder P, Sochet LR. Influence of equivalence ratio on the structure of low-pressure premixed methanol-air flames. Combust Flame 1990;82:163-75.

[223] Akrich R, Vovelle C, Delbourgo R. Flame profiles and combustion mechanisms of methanol-air flames under reduced pressure. Combust Flame 1978;32:171-79.

[224] Bradley D, Dixon-Lewis G, El-Din Habik S, Kwa LK, El-Sherif S. Laminar flame structure and burning velocities of premixed methanol-air. Combust Flame 1991;85:105-20.

[225] Olsson JO, Karlsson LS, Andersson LL. Addition of water to premixed laminar methanol-air flames: Experimental and computational results. J Phys Chem 1986;90:1458-64.

[226] Vandooren J, van Tiggelen PJ. Experimental investigation of methanol oxidation in flames: Mechanisms and rate constants of elementary steps. Proc Combust Inst 1981;18:473-83.

[227] Olsson JO, Olsson IBM, Andersson LL. Lean premixed laminar methanol flames: A computational study. J Phys Chem 1987;91:4160-65.

[228] Norton TS, Dryer FL. The flow reactor oxidation of C_1-C_4 alcohols and MTBE. Proc Combust Inst 1990;23:179-85.

[229] Li J, Zhao Z, Kazakov A, Chaos M, Dryer FL, Scire JJ. A comprehensive kinetic mechanism for CO, CH_2O, and CH_3OH combustion. Int J Chem Kin 2007;39:109-36.

[230] MacLean HL, Lave LB. Evaluating automobile fuel/propulsion system technologies. Prog Energy Combust Sci 2003;29:1-69.

[231] Tanoff MA, Schear DM, Olsson JO, Andersson LA. Combustion of ethanol in laminar flames: Probing with continuous microprobe sampling mass spectrometry. Bull Soc Chim Belg 1992;101:839-50.

[232] Leplat N, Seydi A, Vandooren J. An experimental study of the structure of a stoichiometric ethanol/oxygen/argon flame. Combust Sci Technol 2008;180:519-32.

[233] Dunphy MP, Patterson PM, Simmie JM. High-temperature oxidation of ethanol. Part 2. Kinetic modeling. J Chem Soc Faraday Trans 1991;87:2549-59.

[234] Norton TS, Dryer FL. An experimental and modeling study of ethanol oxidation kinetics in an atmospheric pressure flow reactor. Int J Chem Kin 1992;24:319-44.

[235] Dagaut P, Boettner JC, Cathonnet M. Kinetic modeling of ethanol pyrolysis and combustion. J Chim Phys 1992;89:867-84.

[236] Marinov NM. A detailed chemical kinetic model for high temperature ethanol oxidation. Int J Chem Kin 1999;31:183-220.

[237] Ezeji TC, Qureshi N, Blaschek HP. Bioproduction of butanol from biomass: From genes to bioreactors. Curr Opin Biotech 2007;18:220-27.

[238] Ribeiro NM, Pinto AC, Quintella CM, da Rocha GO, Teixeira LSG, Guarieiro LLN, et al. The role of additives for diesel and diesel blended (ethanol or biodiesel) fuels: A review. Energy Fuels 2007;21:2433-45.

[239] Cool TA, Wang J, Hansen N, Westmoreland PR, Dryer FL, Zhao Z, et al. Photoionization mas spectrometry and modeling studies of the chemistry of fuel-rich dimethyl ether flames. Proc Combust Inst 2007;31:285-93.

[240] Curran HJ, Pitz WJ, Westbrook CK, Dagaut P, Boettner JC, Cathonnet M. A wide range modeling study of dimethyl ether oxidation. Int J Chem Kin 1998;30:229-41.

[241] Fischer SL, Dryer FL, Curran HJ. The reaction kinetics of dimethyl ether. I: High-temperature pyrolysis and oxidation in flow reactors. Int J Chem Kin 2000;32:713-40.

[242] Curran HJ, Fischer SL, Dryer FL. The reaction kinetics of dimethyl ether. II: Low-temperature oxidation in flow reactors. Int J Chem Kin 2000;32:741-59.

[243] Poulopoulos S, Philippopoulos C. Influence of MTBE addition into gasoline on automotive exhaust emissions. Atmos Environ 2000;34:4781-86.

[244] Yao C, Li J, Li Q, Huang C, Wei L, Wang J, et al. Study on combustion of gasoline/MTBE in laminar flame with synchrotron radiation. Chemosphere 2007;67:2065-71.

[245] Werner I, Koger CS, Deanovic LA, Hinton DE. Toxicity of methyl-*tert*-butyl ether to freshwater organisms. Environ Pollut 2001;111:83-88.

[246] McCormick RL, Graboski MS, Alleman TL, Herring AM, Tyson KS. Impact of biodiesel source material and chemical structure on emissions of criteria pollutants from a heavy-duty engine. Environ Sci Technol 2001;35:1742-47.

[247] Oßwald P, Struckmeier U, Kasper T, Kohse-Höinghaus K, Wang J, Cool TA, et al. Isomer-specific fuel destruction pathways in rich flames of methyl acetate and ethyl

formate and consequences for the combustion chemistry of esters. J Phys Chem A 2007;111:4093-101.

[248] Kohse-Höinghaus K, Oßwald P, Struckmeier U, Kasper T, Hansen N, Taatjes CA, et al. The influence of ethanol addition on premixed fuel-rich propene-oxygen-argon flames. Proc Combust Inst 2007;31:1119-27.

[249] Thomas SD, Bhargava A, Westmoreland PR, Lindstedt RP, Skevis G. Propene oxidation chemistry in laminar premixed flames. Bull Soc Chim Belg 1996;105:501-12.

[250] Walravens B, Vandooren J, van Tiggelen PJ. Peculiar features in lean butane flames. Combust Sci Technol 1997;130:399-409.

[251] Douté C, Delfau JL, Akrich R, Vovelle C. Experimental study of the chemical structure of low-pressure premixed *n*-heptane-O_2-Ar and iso-octane-O_2-Ar flames. Combust Sci Technol 1997;124:249-76.

[252] Douté C, Delfau JL, Vovelle C. Detailed reaction mechanisms for low pressure premixed *n*-heptane flames. Combust Sci Technol 1999;147:61-109.

[253] Safieh HY, Vandooren J, van Tiggelen PJ. Experimental study of inhibition induced by CF_3Br in a CO-H_2-O_2-Ar flame. Proc Combust Inst 1982;19:117-26.

[254] Wang T, Li S, Lin Z, Han D, Han X. Experimental study of laminar lean premixed methylmethacrylate/oxygen/argon flame at low pressure. J Phys Chem A 2008;112:1219-27.

[255] Tian Z, Li Y, Zhang T, Zhu A, Cui Z, Qi F. An experimental study of low-pressure premixed pyrrole/oxygen/argon flames with tunable synchrotron photoionization. Combust Flame 2007;151:347-65.

[256] El Bakali A, Dupont L, Lefort B, Lamoureux N, Pauwels JF, Montero M. Experimental study and detailed modeling of toluene degradation in a low-pressure stoichiometric premixed $CH_4/O_2/N_2$ flame. J Phys Chem A 2007;111:3907-21.

[257] Shandross RA, Longwell JP, Howard JB. Destruction of benzene in high-temperature flames: Chemistry of benzene and phenol. Proc Combust Inst 1996;26:711-19.

Table 1:

List of selected studies reporting flame-sampling molecular-beam mass spectrometric measurements of premixed laminar low-pressure flames

Fuel (IUPAC)	Stoichiometry ϕ (Pressure/Torr)	Method	Reference
	Hydrocarbon Fuels		
Methane (CH_4)	1.00 (20)	EI	[181]
	0.92 (20), 1.17 (20), 1.42 (30), 1.68 (40), 1.94 (60)	EI	[132]
	1.60 (31)	EI	[178]
	0.69 (40), 1.00 (40), 1.18 (40)	EI	[182, 183]
Acetylene (C_2H_2)	1.93 (37.5)	EI	[77, 184]
	2.40 (20)	EI	[153, 191]
	1.00 (15), 1.50 (15), 2.00 (20), 2.25 (26)	EI	[133]
	2.50 (20)	EI	[188]
	2.60 (20)	EI	[185]
Ethylene (C_2H_4)	0.70 (30)	EI	[174]
	1.00 (20)	VUV PI	[165]
	1.00 (22.5), 1.25 (26.25), 1.50 (30), 1.75 (37.5), 2.0 (37.5)	EI	[186]
	0.75 (30)	EI	[55]
	1.90 (20)	EI	[130]
	1.8 (20), 2.0 (20), 2.1 (20), 2.2 (20), 2.6 (20), 3.0 (20)	EI	[193]
Ethane (C_2H_6)	1.00 (20)	EI	[181]
	1.00 (15), 1.50 (20), 2.00 (50), 2.25 (70)	EI	[134]
	1.00 (40)	EI	[182, 183]

Allene (C_3H_4)	1.8 (25)	VUV PI	[128, 145, 166, 169]
Propyne (C_3H_4)	1.8 (25)	VUV PI	[128, 145, 166, 169]
Propene (C_3H_6)	1.80 (37.5), 2.33 (37.5)	EI	[68, 77, 184, 189, 248
	2.33 (37.5)	REMPI	[74]
	0.23 (30)	EI	[249]
Propane (C_3H_8)	1.8 (30)	VUV PI	[105]
1,3-Butadiene (C_4H_6)	2.4 (20)	EI	[150]
Butane (C_4H_{10})	0.21 (25.3)	EI	[250]
iso-Butane (C_4H_{10})	0.21 (25.3)	EI	[250]
1,3-Pentadiene (C_5H_8)	2.16 (37.5)	EI	[201]
Cyclopentene (C_5H_8)	1.68 (37.5), 2.16 (37.5), 2.63 (37.5)	EI	[77, 199]
	2.16 (37.5)	REMPI	[74]
	2.0 (37.5)	VUV PI	[104, 128, 142, 145, 1
1-Pentene (C_5H_{10})	2.32 (37.5)	EI	[77, 197]
Benzene (C_6H_6)	1.0 (20)	REMPI	[76]
	1.66 (35)	VUV PI	[123, 128, 145]
	1.78 (30)	VUV PI	[164]
	1.8 (20)	EI	[54]
	2.0 (37.5)	EI	[215]
	2.4 (40)	EI	[216]
Cyclohexane (C_6H_{12})	1.0 (30)	VUV PI / EI	[202]
n-Heptane (C_7H_{16})	0.7 (45), 1.0 (45), 1.5 (45), 2.0 (45)	EI	[251, 252]
iso-Octane (C_8H_{18})	0.7 (45), 1.0 (45), 1.5 (45), 2.0 (45)	EI	[251]
	Oxygenated Fuels		
Carbon Monoxide (CO)	1.00 (50)	EI	[253]

Formaldehyde (CH_2O)	0.22 (22.5)	EI	[131]
Acetone (C_2H_6O)	0.76 (15), 1.83 (30)	VUV PI	[173]
Methanol (CH_4O)	0.36 (40), 0.89 (40)	EI	[226]
Ethanol (C_2H_6O)	1.00 (37.5), 2.57 (37.5) 1.00 (37.5)	REMPI / EI EI	[75] [232]
1-Propanol (C_3H_8O)	0.75 (15), 1.80 (30)	VUV PI	[173]
2-Propanol (C_3H_8O)	0.75 (15), 1.80 (30)	VUV PI	[173]
1-Butanol ($C_4H_{10}O$)	1.71 (30)	VUV PI	[172]
2-Butanol ($C_4H_{10}O$)	1.71 (30)	VUV PI	[172]
iso-Butanol ($C_4H_{10}O$)	1.71 (30)	VUV PI	[172]
tert-Butanol ($C_4H_{10}O$)	1.71 (30)	VUV PI	[172]
Dimethyl ether (DME) (C_2H_6O)	0.98 (30), 1.20 (30) 1.2 (30), 1.68 (20)	VUV PI / EI VUV PI	[86] [239]
Methyl *tert*-butyl ether (MTBE) ($C_5H_{12}O$)	0.18 (30), 1.00 (30), 1.84 (30)	EI	[135]
Methylacetate ($C_3H_6O_2$)	1.82 (30)	VUV PI	[247]
Ethylformate ($C_3H_6O_2$)	1.82 (30)	VUV PI	[247]
Methylmethacrylate ($C_5H_8O_2$)	0.75 (20)	VUV PI	[254]
	Nitrogen Containing Fuel		
Pyrrole (C_4H_5N)	0.55 (25), 1.84 (25)	VUV PI	[255]
	Fuel Mixtures		
Methane/N_2 (CH_4/N_2)	1.0 (39)	EI	[256]
Methane/Toluene/N_2 ($CH_4/C_7H_8/N_2$)	1.0 (39)	EI	[256]

1,3-Butadiene/H_2 (C_4H_6/H_2)	1.44 (30)	VUV PI	[87]
Butane/H_2 (C_4H_{10}/H_2)	0.17 (20.3)	EI	[250]
iso-Butane/H_2 (C_4H_{10}/H_2)	0.17 (20.3)	EI	[250]
Benzene/H_2 (C_6H_6/H_2)	1.79 (22)	EI	[257]
Ethylene/Allene (C_2H_4/C_3H_4)	0.69 (30)	VUV PI / EI	[174]
Acetylene/Propene (C_2H_2/C_3H_6)	2.16 (37.5)	EI	[201]
Methanol/H_2 (CH_4O/H_2)	0.21 (40)	EI	[226]
Methanol/N_2 (CH_4O/N_2)	1.00 (100)	EI	[225]
Propene/Ethanol (C_3H_6/C_2H_6O)	*C/O = 0.77:* 2.35 (37.5), 2.37 (37.5), 2.38 (37.5), 2.40 (37.5), 2.42 (37.5) *C/O = 0.60:* 1.83 (37.5), 1.85 (37.5), 1.86 (37.5), 1.88 (37.5), 1.93 (37.5), 1.98 (37.5), 2.12 (37.5), 2.30 (37.5)	VUV PI / EI / REMPI EI / REMPI	[75, 248] [75]
Gasoline	0.75 (15), 1.73 (30)	VUV PI	[170, 171]
Gasoline/MTBE		VUV PI	[244]

Figure Captions:

Figure 1:

Photograph and schematic structure of a flat premixed laminar low-pressure flame. Temperature and mole fractions of reactions, products, and intermediate species are given as function of height above the burner. In the photograph, a widespread reaction (luminous) flame zone and the quartz nozzle used for molecular beam sampling are seen as well.

Figure 2:

Schematic diagram of an experimental setup for molecular beam sampling in low pressure flames.

Figure 3:

Illustration of different ionization techniques: a) Electron Ionization, b) Resonantly Enhanced Multi-Photon Ionization (REMPI), and c) VUV Single-Photon Ionization. See text for further details.

Figure 4:

Mole fraction profile of benzene in a fuel-rich propene flame measured with flame-sampling molecular-beam mass spectrometry employing electron ionization (EI), resonantly enhanced multi-photon ionization (REMPI), and single-photon ionization.

Figure 5:

2+1 REMPI spectrum of *m/z* = 92 in a fuel-rich propene flame (upper trace) and a toluene cold gas flow (lower trace). The inset shows a UV absorption spectrum of toluene vapor. Figure is from [78].

Figure 6:

Time-of-flight mass spectrum recorded with photons of 11.1 eV at 2.75 mm distance from the burner in a fuel-rich cyclopentene-O_2 flame. All peaks are easily assigned to various common combustion intermediates.

Figure 7:

(a) Electron ionization cross section of propane (C_3H_8) at electron energy of 8-20 eV. Data from Refs. [106, 107] and calculated using the BEB method are compared with experimental ion signal data. In addition, contributions from fragment ions are shown. (b) Photoionization cross section from 10.5-12.5 eV. Partial cross sections of individual fragment ions are shown together with the total cross section.

Figure 8:

The flame-sampling photoionization molecular-beam mass spectrometer for use with synchrotron generated VUV photon beams. The burner can be translated along the molecular-beam axis to sample flame species at various distances from the burner face. Typical flame pressures and orifice diameters of the quartz probe are 20-40 Torr and ~300 μm, respectively. Turbo pumps keep the pressures in the first stage, the ionization chamber, and the vertically

aligned flight tube below 10^{-4}, 10^{-6}, and 10^{-7} Torr, respectively. Ions are detected using a multichannel plate (MCP) detector.

Figure 9:

A flame-sampled photoionization efficiency spectra for *m/z* = 40 as sampled from a rich cyclopentene-O_2 flame and the comparison with cold-flow photoioinization efficiency spectra of allene and propyne. Both C_3H_4 isomers are easily identified. The inset shows the isomerically resolved C_3H_4 mole fraction profiles for the same flame.

Figure 10:

(a) Number of total conceivable isomers of the hydrocarbons with the general structure C_xH_y. Only closed-shell molecules are considered and cyclic species are taken into account only for four-membered rings or bigger. (b) Ionization of several isomers or near-equal mass species between *m/z* = 40 and *m/z* = 80. The specific ionization energies can be used to identify the species and to perform concentration measurements independently from each other.

Figure 11:

Molecular structures of selected isomers of C_3H_2, C_4H_3, C_4H_5, C_5H_3, and C_5H_5. For resonantly stabilized isomers, only one possible electronic structure is shown.

Figure 12:

Possible product formation of reactions between cyclopentadienyl (C_5H_5) with acetylene (C_2H_2). (a) The initial adduct undergoes a 1,3-H shift and H-atom elimination to form the $C_5H_4CCH_2$, or

(b) it undergoes H-atom elimination and subsequent H-atom migration. (c) In a ring-opening reaction it may form cycloheptatrienyl which can isomerize to form benzyl.

Figure 13:

Isomer-specific differences in flames fueled by the C_3H_4 isomers allene (left column) and propyne (right column). Mole fraction profiles of the main species (H_2, H_2O, CO, O_2, fuel, Ar, CO_2) are shown in (a) for the allene flame and in (b) for the propyne flame. Little or no differences are observed between the flames fueled by the C_3H_4 isomers. (c) Mole fraction profiles of propyne and propargyl in the allene flame and (d) mole fraction profiles of allene and propargyl in the propyne flame. Propyne is more pronounced in the allene flame than allene in the propyne flame. More propargyl is formed in the allene flame than it is the propyne flame. (e) The experimentally observed and modeled C_6H_6 profile in the allene flame is compared with (f) the somewhat lower mole fraction of C_6H_6 in the propyne flame. Symbols denote experimental results, while modeling results are represented by solid lines.

Figure 14:

Formation of benzene from cyclohexane via cyclohexene and 1,3-cyclohexadiene and the respective radical intermediates.

Figure 15:

Early reaction pathways in the combustion of ethanol. Abstractions of hydrogen atoms lead to three different C_2H_5O radicals and subsequent β-scissions form ethene, ethenol, acetaldehyde, and formaldehyde.

Figure 16:

Experimental (lines and symbols) and modeled (lines) mole fraction profiles of (a) CH_2O, C_2H_6, C_2H_4, and C_2H_2 and (b) CH_4, CH_3, and HCO in a fuel-rich (ϕ = 1.20) low-pressure dimethyl ether flame. A very good agreement between experimental data and kinetic model is observed. (c) Schematic diagram of the key reaction pathways.

Figure 17:

Experimental mole fraction profiles of C_2H_4, C_2H_2, H_2CO, and CH_3CHO in fuel-rich (ϕ = 1.82) low-pressure flames fueled by the structural isomers ethylformate ($HCOOC_2H_5$) and methylacetate (CH_3COOCH_3).[247]

Figure 1:

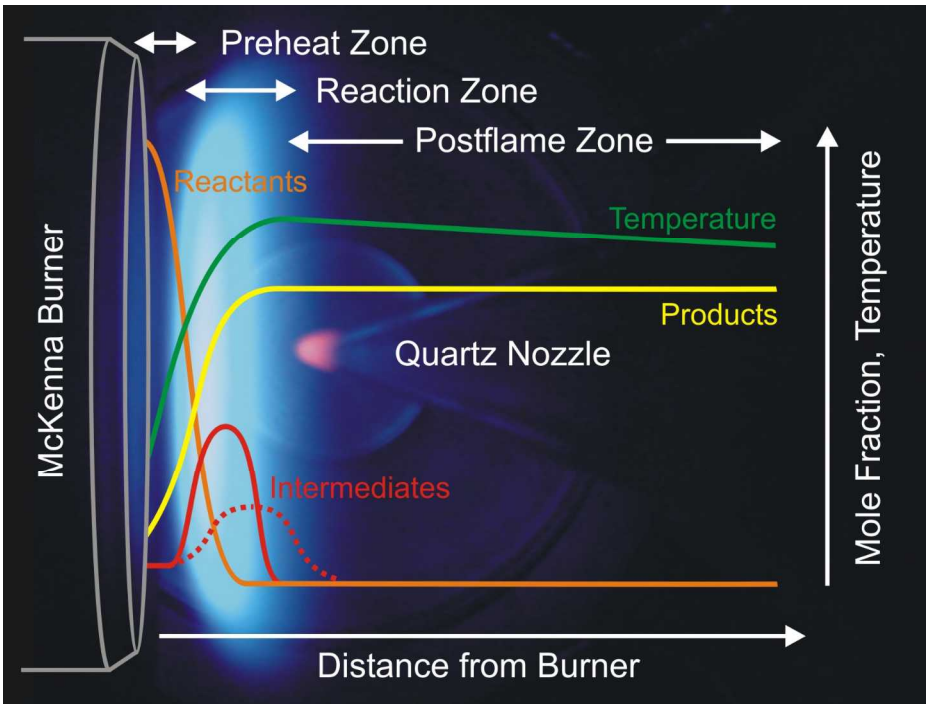
Preheat Zone
Reaction Zone
Postflame Zone
Reactants
Temperature
Products
Quartz Nozzle
Intermediates
McKenna Burner
Mole Fraction, Temperature
Distance from Burner

Figure 2:

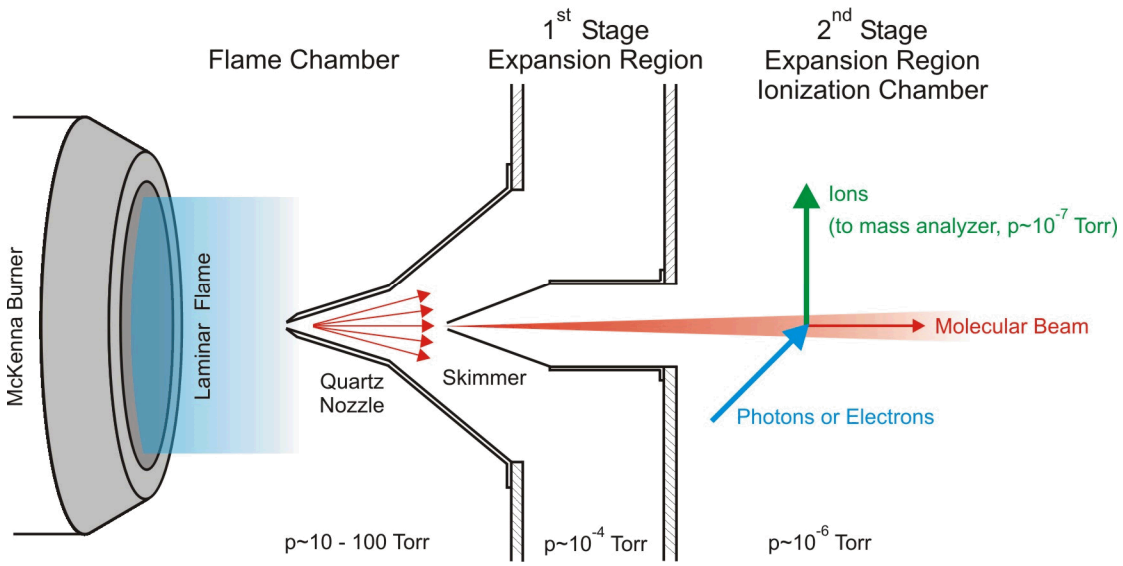
Flame Chamber
1st Stage
Expansion Region
2nd Stage
Expansion Region
Ionization Chamber
McKenna Burner
Laminar Flame
Quartz
Nozzle
Skimmer
Ions
(to mass analyzer, p~10-7 Torr)
Molecular Beam
Photons or Electrons
p~10 - 100 Torr
p~10-4 Torr
p~10-6 Torr

Figure 3:

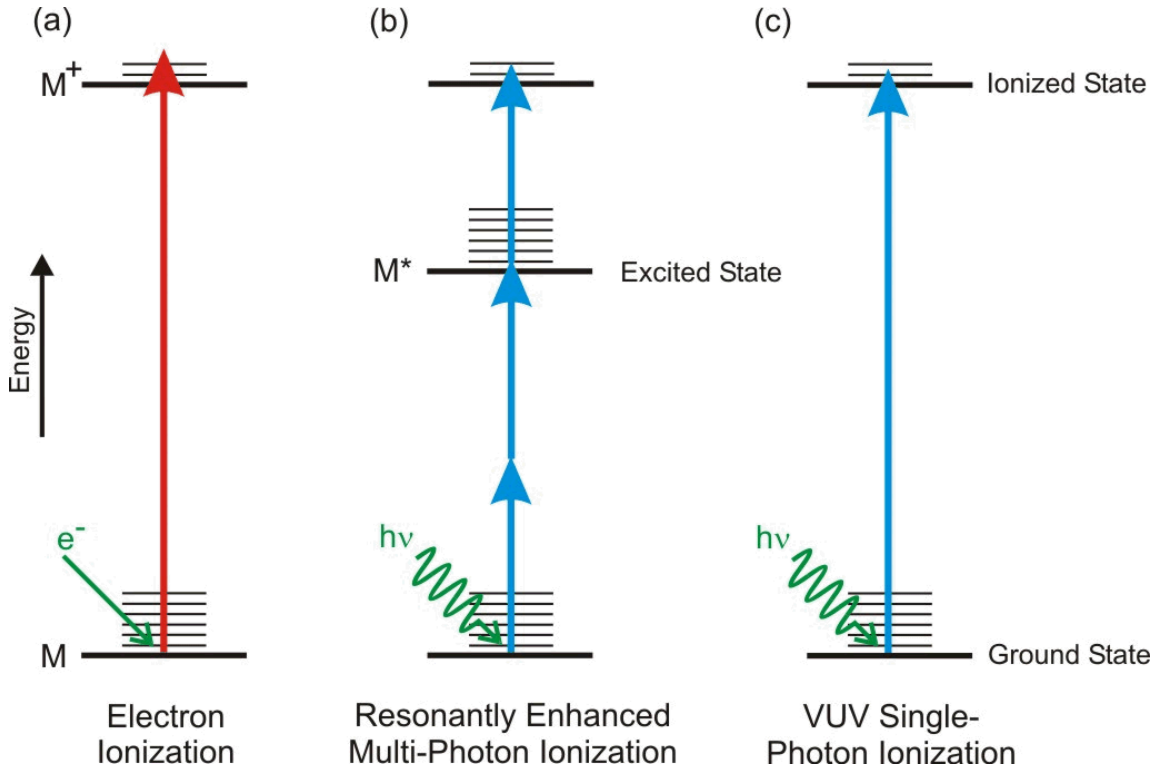
(a)
(b)
(c)
M+
Energy
e-
M
M*
Excited State
hν
hν
Ionized State
Ground State
Electron Ionization
Resonantly Enhanced Multi-Photon Ionization
VUV Single-Photon Ionization

Figure 4:

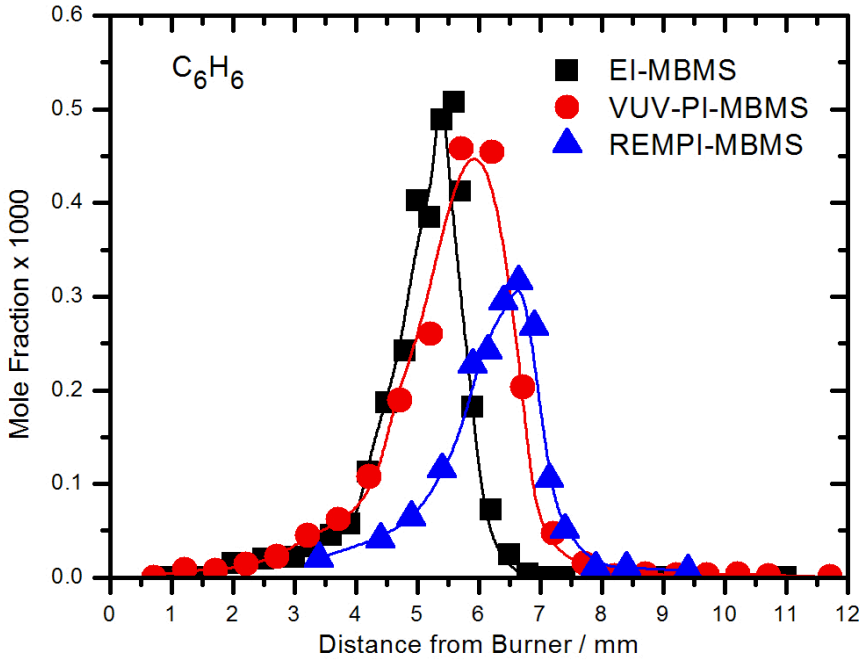
C6H6
EI-MBMS
VUV-PI-MBMS
REMPI-MBMS
Mole Fraction x 1000
Distance from Burner / mm
0.0
0.1
0.2
0.3
0.4
0.5
0.6
0
1
2
3
4
5
6
7
8
9
10
11
12

Figure 5:

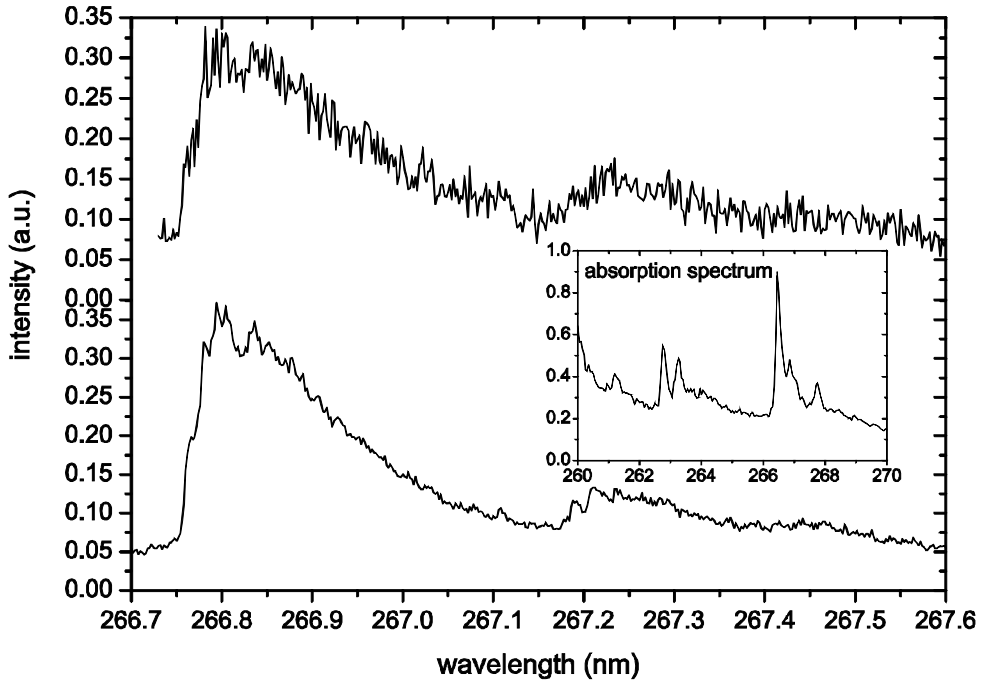

Figure 6:

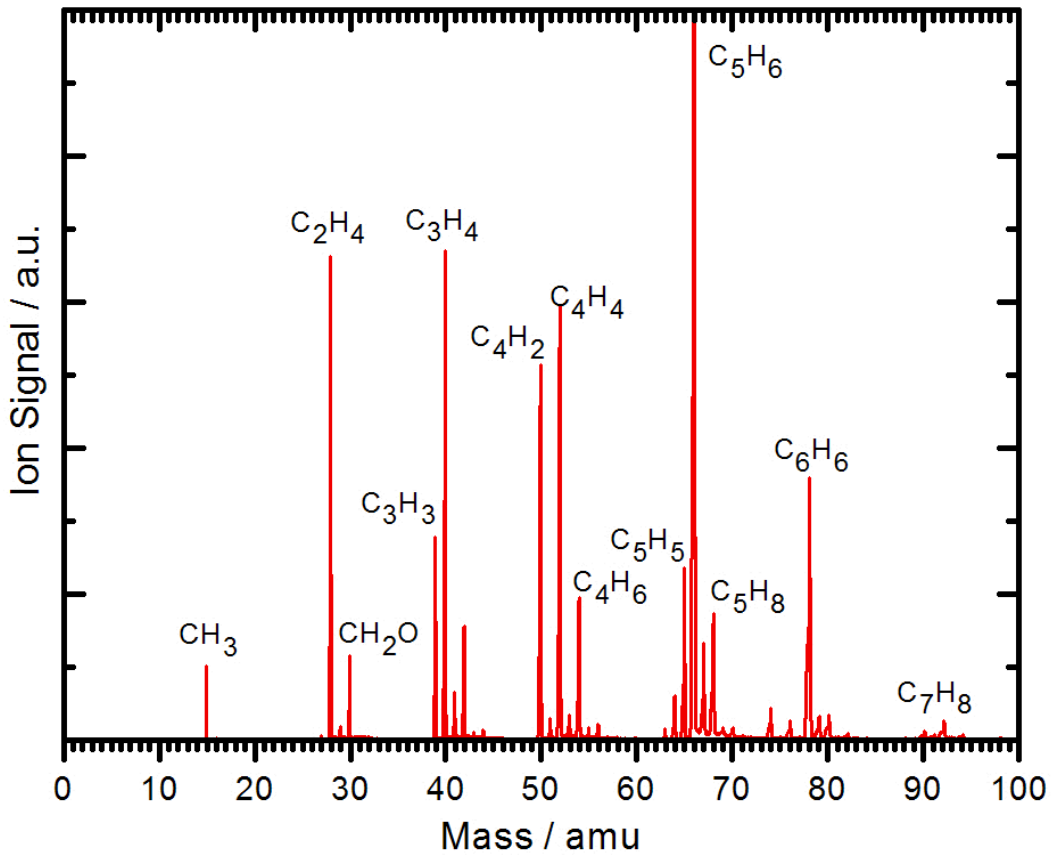
Ion Signal / a.u.
Mass / amu
0
10
20
30
40
50
60
70
80
90
100
C_5H_6
C_2H_4
C_3H_4
C_4H_4
C_4H_2
C_6H_6
C_3H_3
C_5H_5
C_4H_6
C_5H_8
CH_3
CH_2O
C_7H_8

Figure 7:

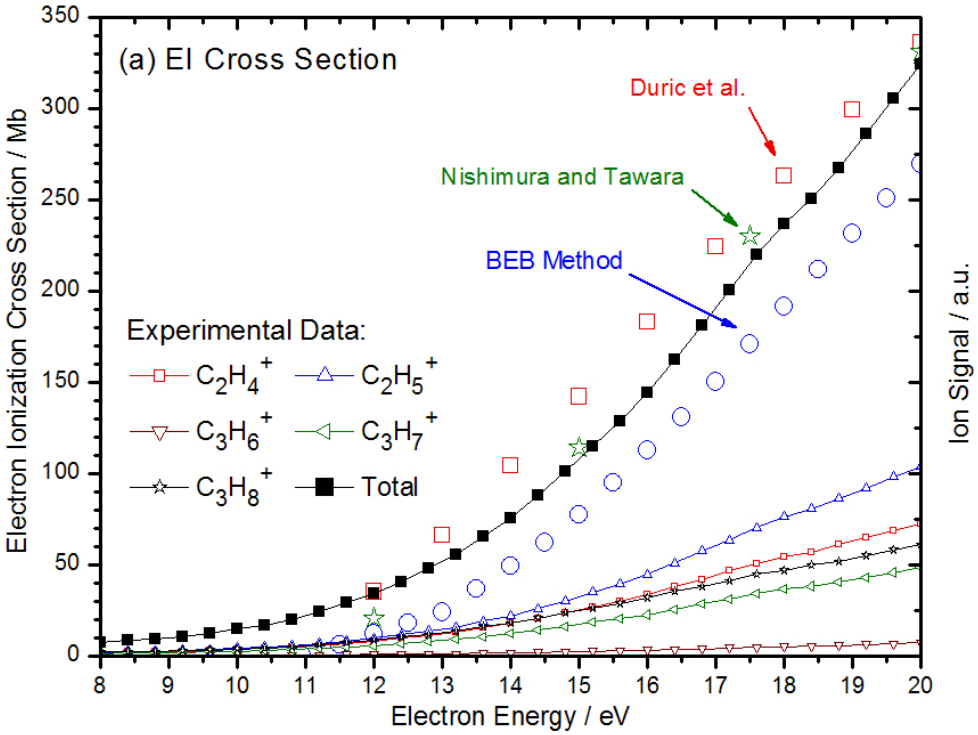
(a) EI Cross Section
Duric et al.
Nishimura and Tawara
BEB Method
Experimental Data:
$C_2H_4^+$
$C_2H_5^+$
$C_3H_6^+$
$C_3H_7^+$
$C_3H_8^+$
Total
Electron Ionization Cross Section / Mb
Ion Signal / a.u.
Electron Energy / eV

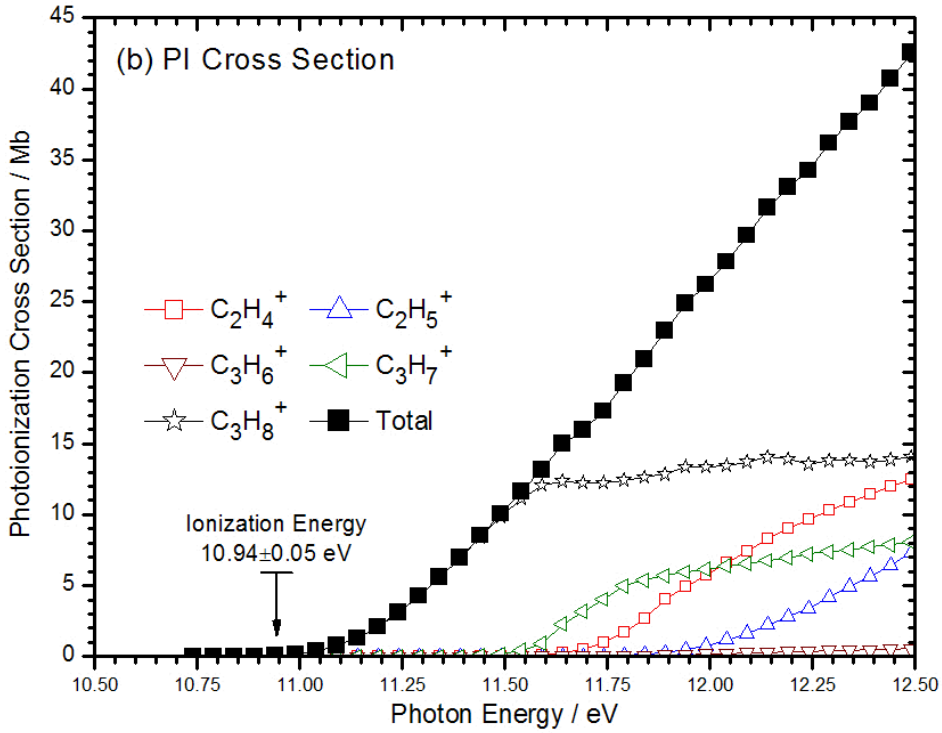
(b) PI Cross Section
$C_2H_4^+$
$C_2H_5^+$
$C_3H_6^+$
$C_3H_7^+$
$C_3H_8^+$
Total
Ionization Energy
10.94±0.05 eV
Photoionization Cross Section / Mb
Photon Energy / eV

Figure 8:

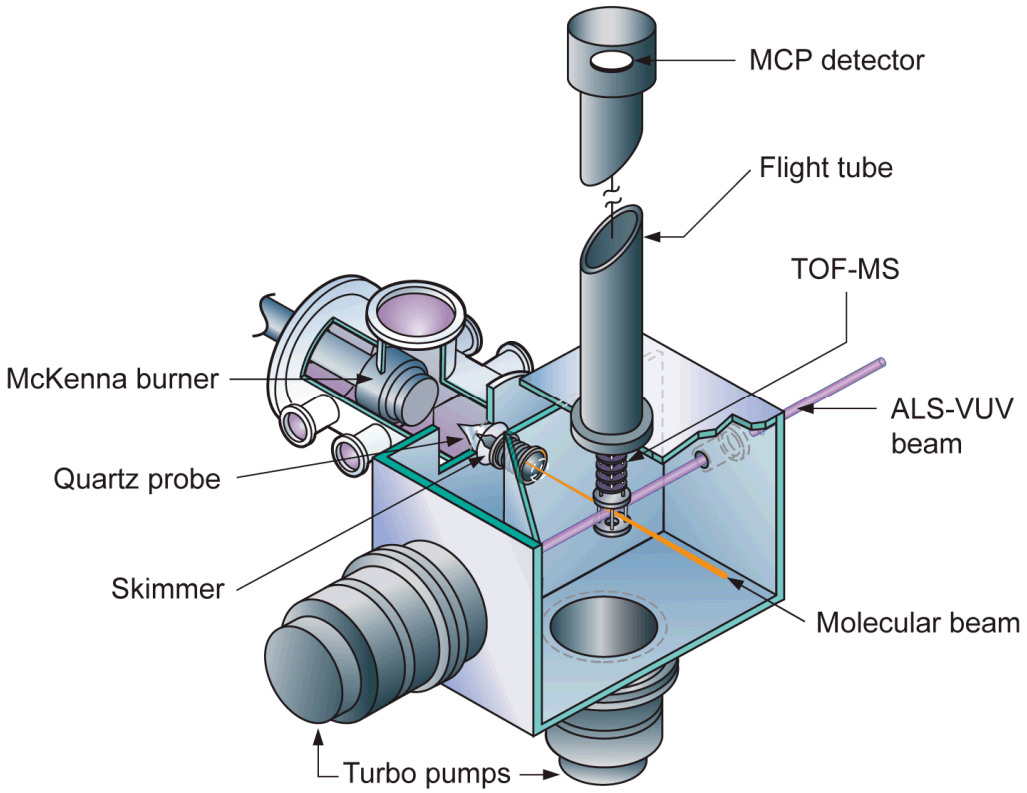
MCP detector
Flight tube
TOF-MS
McKenna burner
ALS-VUV beam
Quartz probe
Skimmer
Molecular beam
Turbo pumps

Figure 9:

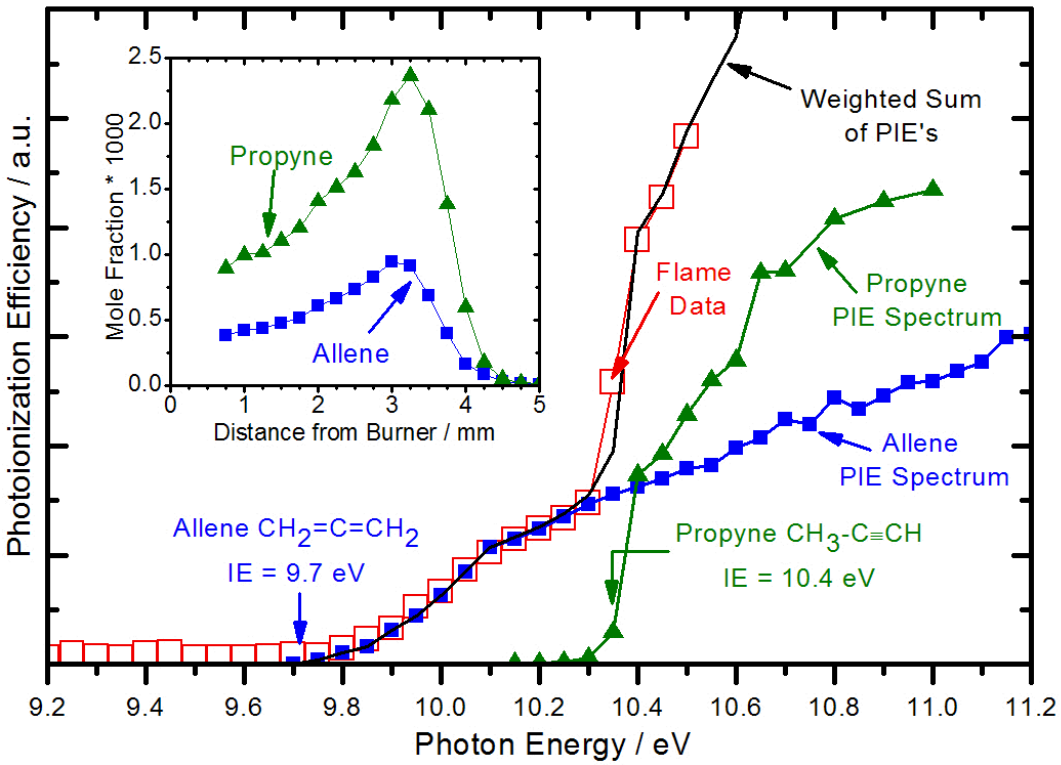
Photoionization Efficiency / a.u.
Photon Energy / eV
Mole Fraction * 1000
Distance from Burner / mm
Propyne
Allene
Weighted Sum of PIE's
Flame Data
Propyne PIE Spectrum
Allene PIE Spectrum
Allene CH2=C=CH2
IE = 9.7 eV
Propyne CH3-C≡CH
IE = 10.4 eV

Figure 10:

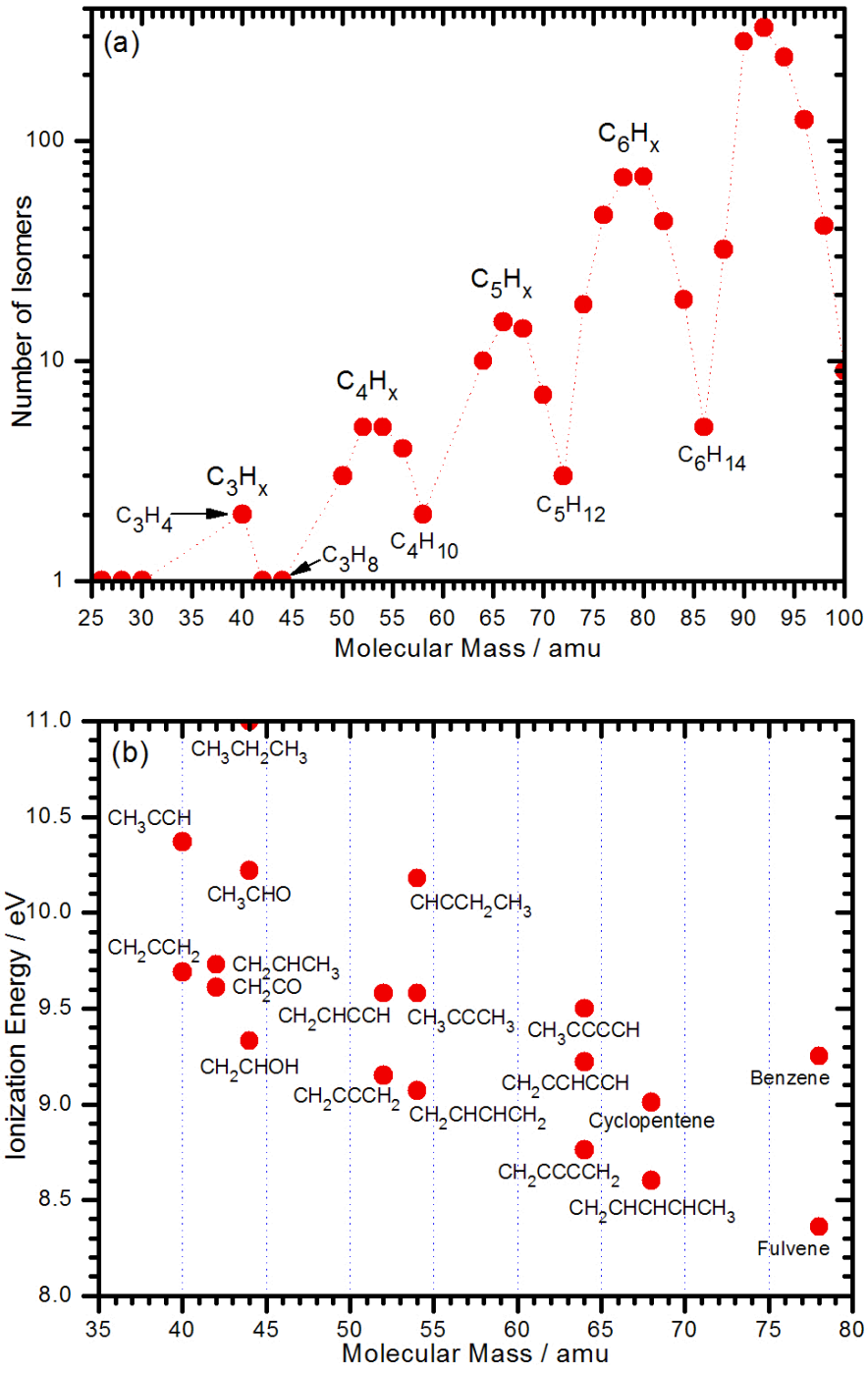
(a)
Number of Isomers
Molecular Mass / amu
C_3H_x
C_3H_4
C_3H_8
C_4H_x
C_4H_{10}
C_5H_x
C_5H_{12}
C_6H_x
C_6H_{14}
(b)
Ionization Energy / eV
Molecular Mass / amu
$CH_3CH_2CH_3$
CH_3CCH
CH_3CHO
$CHCCH_2CH_3$
CH_2CCH_2
CH_2CHCH_3
CH_2CO
CH_2CHCCH
CH_3CCCH_3
CH_3CCCCH
CH_2CHOH
CH_2CCHCH
CH_2CCCH_2
$CH_2CHCHCH_2$
Cyclopentene
Benzene
CH_2CCCCH_2
$CH_2CHCHCHCH_3$
Fulvene

Figure 11:

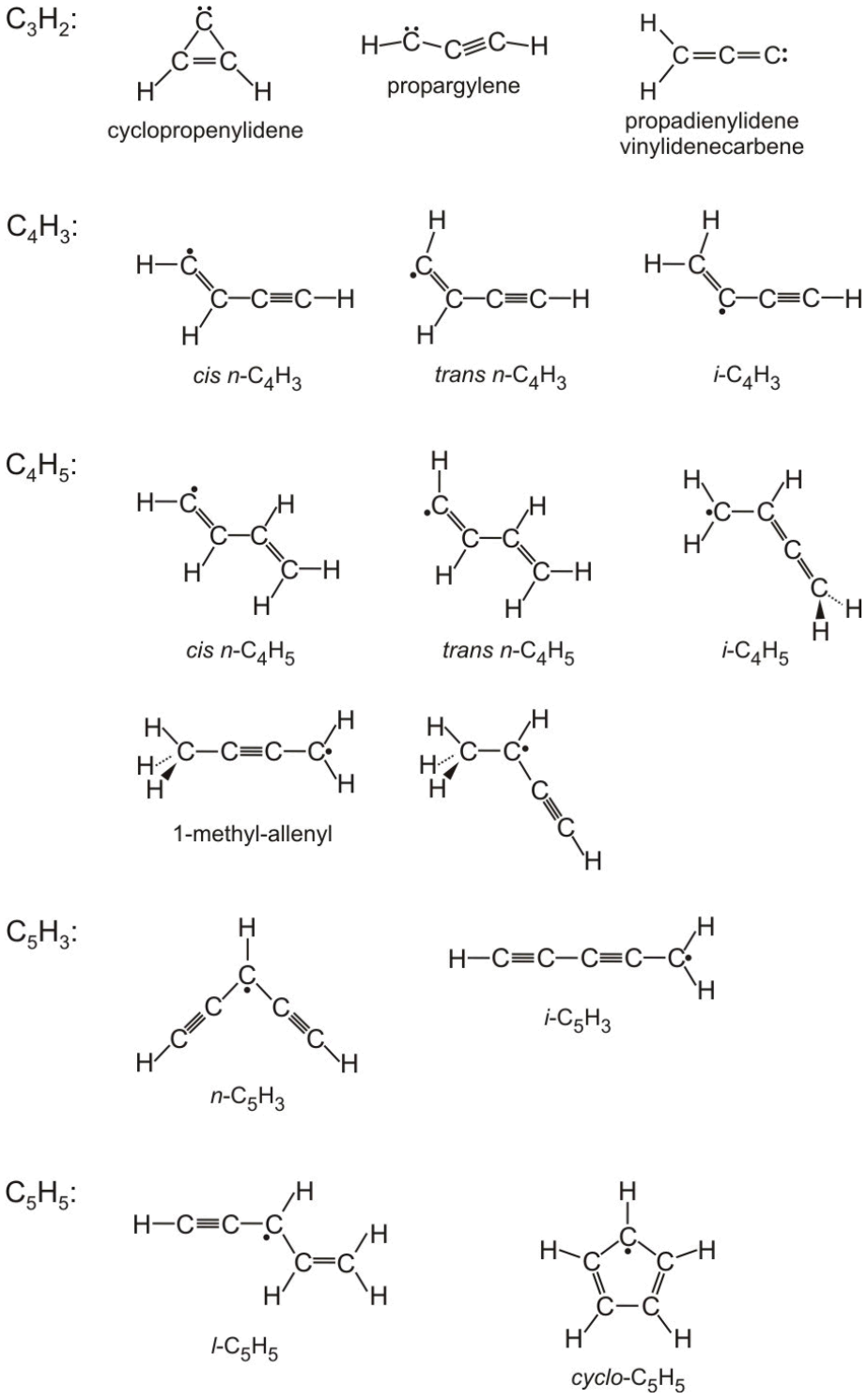
C3H2:
cyclopropenylidene
propargylene
propadienylidene
vinylidenecarbene
C4H3:
cis n-C4H3
trans n-C4H3
i-C4H3
C4H5:
cis n-C4H5
trans n-C4H5
i-C4H5
1-methyl-allenyl
C5H3:
n-C5H3
i-C5H3
C5H5:
l-C5H5
cyclo-C5H5

Figure 12:

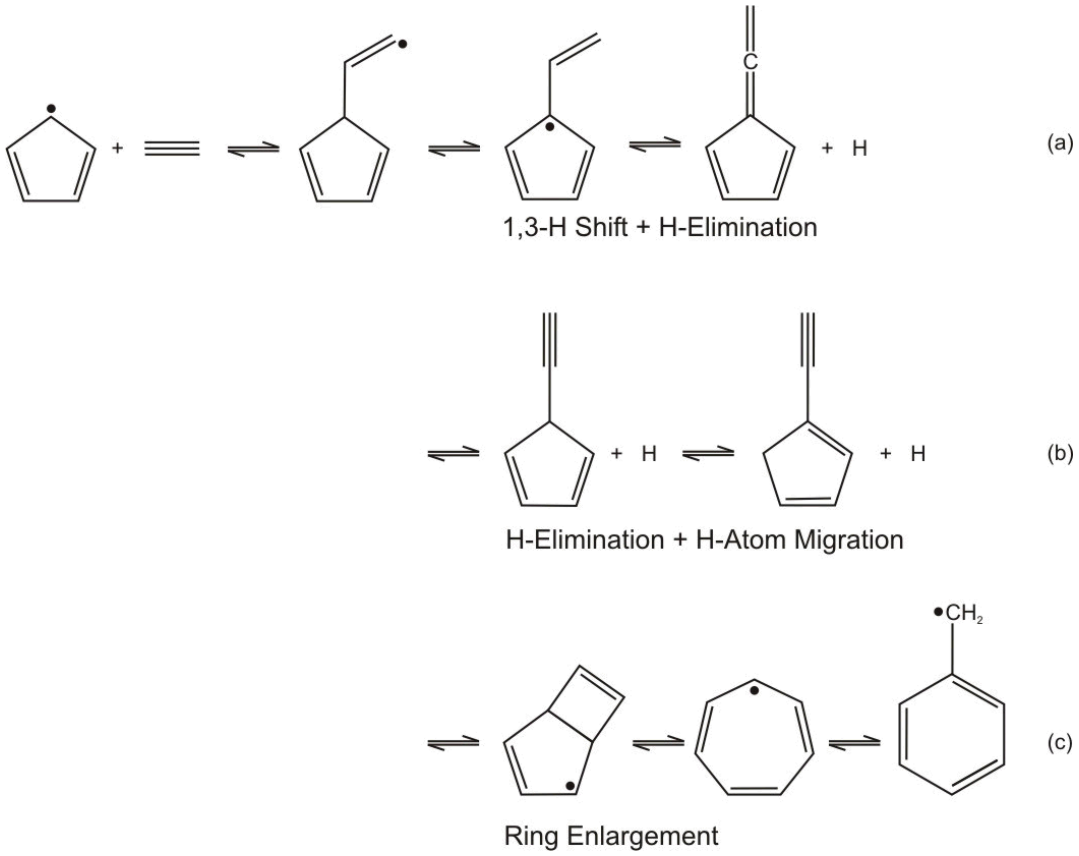
C
+ H
(a)
1,3-H Shift + H-Elimination
+ H
+ H
(b)
H-Elimination + H-Atom Migration
•CH2
(c)
Ring Enlargement

Figure 13:

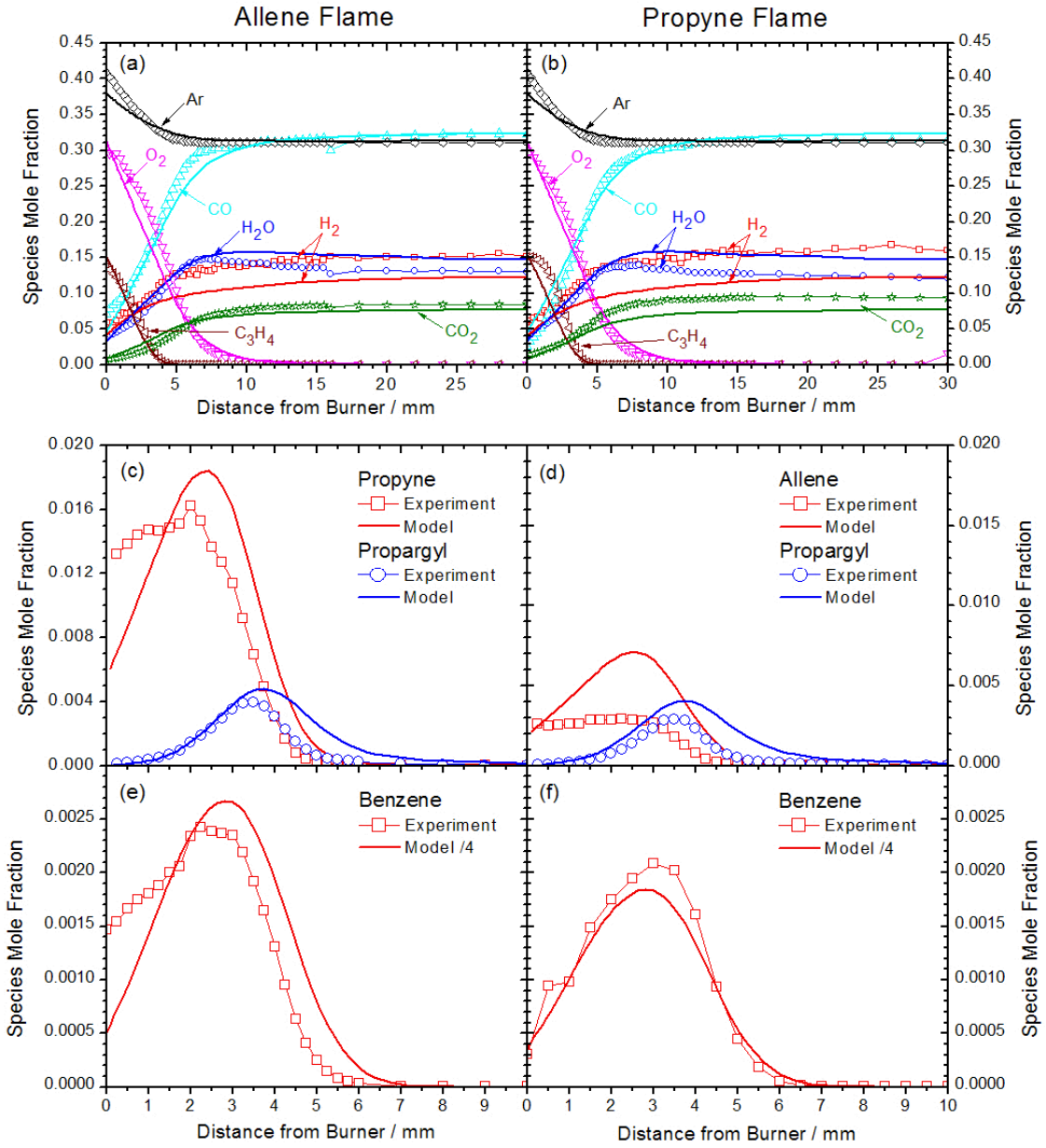
Allene Flame
Propyne Flame
(a)
(b)
(c)
(d)
(e)
(f)
Ar
O2
CO
H2O
H2
C3H4
CO2
Species Mole Fraction
Distance from Burner / mm
Propyne
Allene
Propargyl
Benzene
Experiment
Model
Model /4

Figure 14:

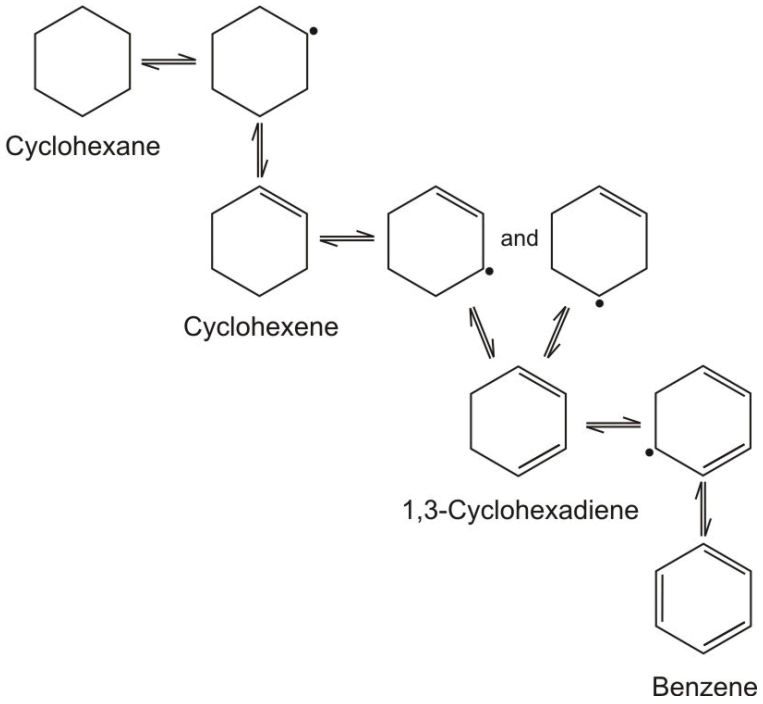

Figure 15:

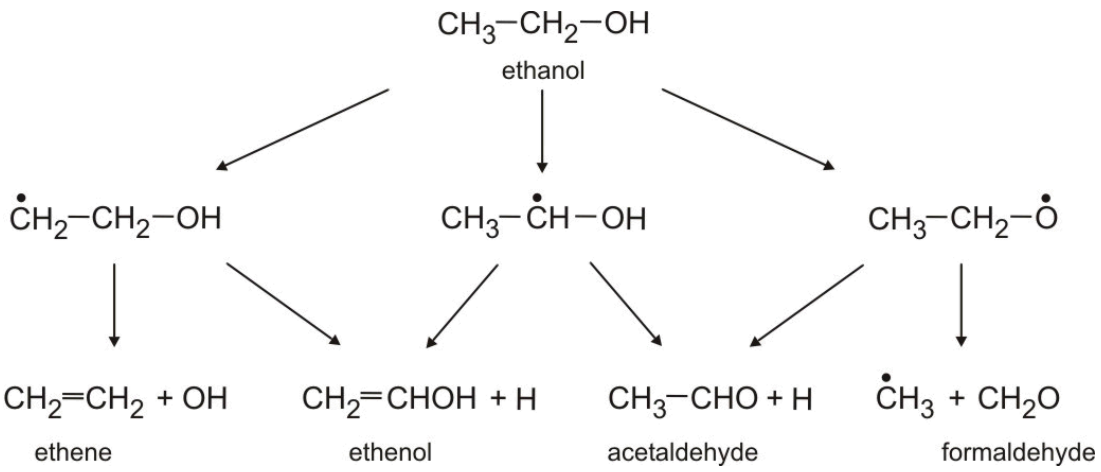
CH3–CH2–OH
ethanol
•CH2–CH2–OH
CH3–•CH–OH
CH3–CH2–O•
CH2=CH2 + OH
ethene
CH2=CHOH + H
ethenol
CH3–CHO + H
acetaldehyde
•CH3 + CH2O
formaldehyde

Figure 16:

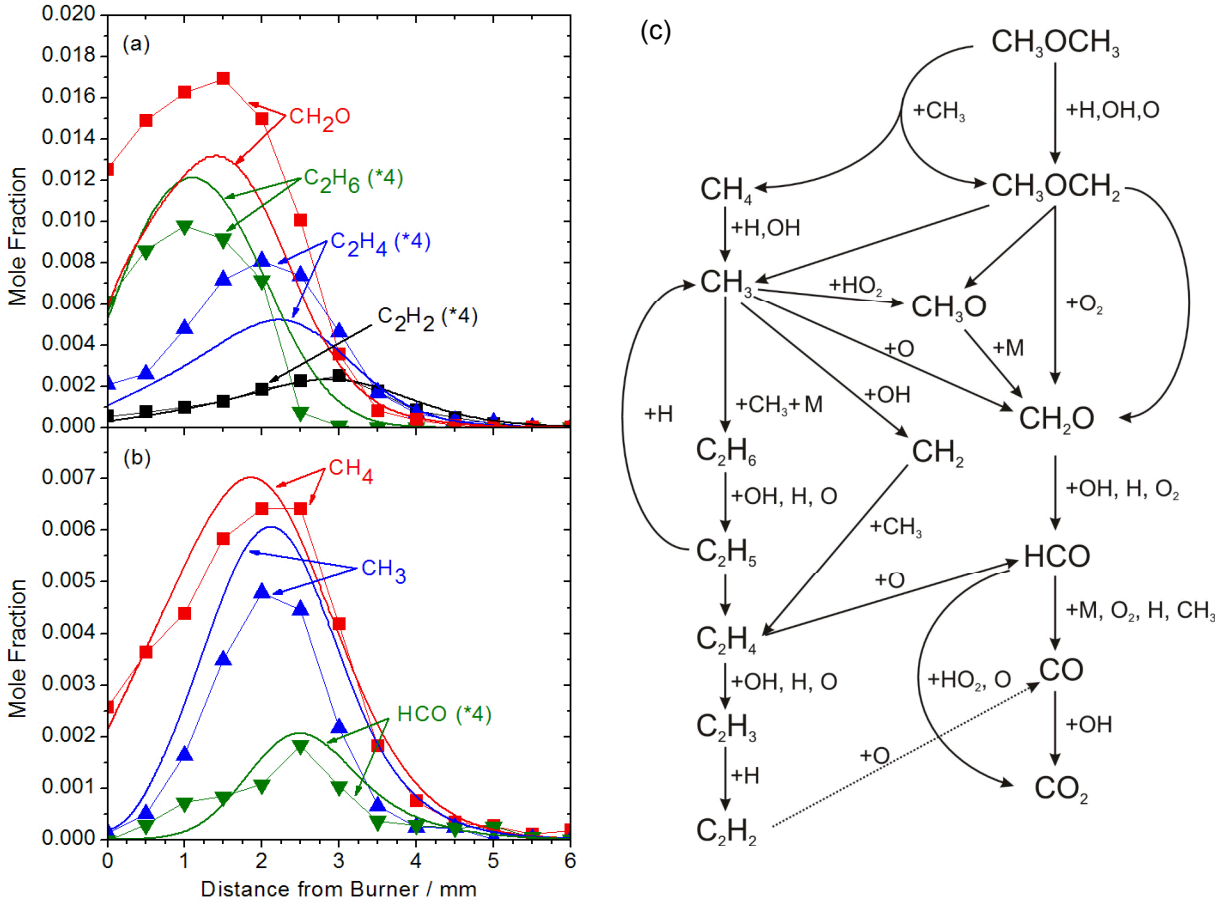
(a)
(b)
(c)
Mole Fraction
Distance from Burner / mm
CH2O
C2H6 (*4)
C2H4 (*4)
C2H2 (*4)
CH4
CH3
HCO (*4)
CH3OCH3
CH3OCH2
CH3O
CH2O
C2H6
C2H5
C2H4
C2H3
C2H2
CH2
HCO
CO
CO2
+CH3
+H,OH,O
+H,OH
+HO2
+O2
+O
+M
+H
+CH3+M
+OH
+OH, H, O
+OH, H, O2
+CH3
+M, O2, H, CH3
+HO2, O

Figure 17:

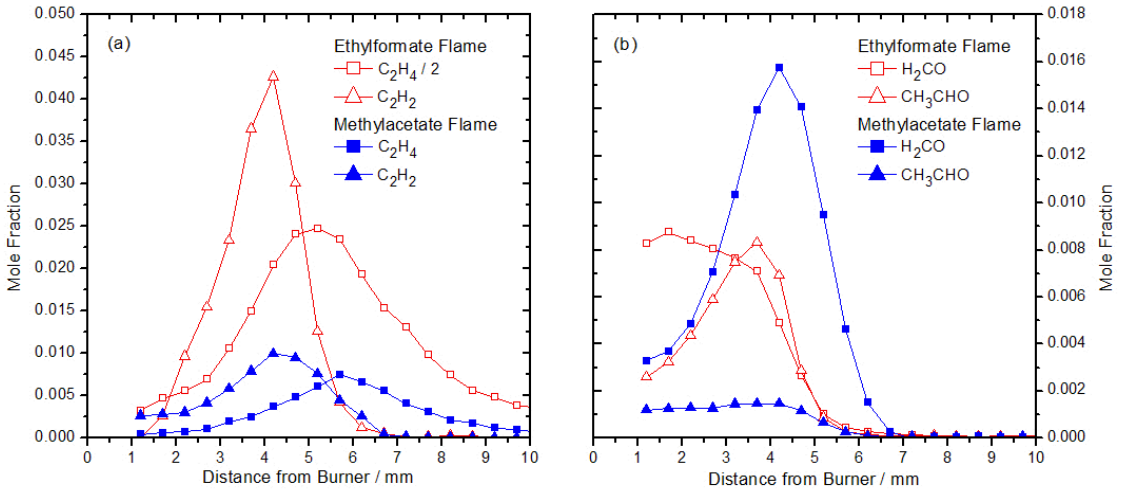
(a)
Ethylformate Flame
C_2H_4 / 2
C_2H_2
Methylacetate Flame
C_2H_4
C_2H_2
Mole Fraction
Distance from Burner / mm
(b)
Ethylformate Flame
H_2CO
CH_3CHO
Methylacetate Flame
H_2CO
CH_3CHO
Mole Fraction
Distance from Burner / mm